New push-pull dyes based on 2-(3-oxo-2,3-dihydro-1H-cyclopenta[b]naphthalen-1-ylidene)malononitrile: An amine-directed synthesis

Corentin Pigot, Guillaume Noirbent, Sebastien Peralta, Sylvain Duval, Thanh-Tuan Bui, Pierre-Henri Aubert, Malek Nechab, Didier Gigmes, Frederic Dumur

Contents lists available at ScienceDirect

Dyes and Pigments

journal homepage: http://ees.elsevier.com

New push-pull dyes based on 2-(3-oxo-2,3-dihydro-1*H*-cyclopenta[*b*]naphthalen-1-ylidene)malononitrile: An amine-directed synthesis

Corentin Pigot [a,**], Guillaume Noirbent [a], Sébastien Peralta [b], Sylvain Duval [c], Thanh-Tuan Bui [b], Pierre-Henri Aubert [b], Malek Nechab [a], Didier Gigmes [a], Frédéric Dumur [a,*]

[a] *Aix Marseille Univ, CNRS, ICR UMR 7273, F-13397, Marseille, France*
[b] *Laboratoire de Physicochimie des Polymères et des Interfaces (LPPI), Université de Cergy Pontoise, 5 Mail Gay Lussac, F-95000, Neuville-sur-Oise, France*
[c] *Université de Lille, CNRS, Centrale Lille, ENSCL, Univ. Artois, UMR 8181 - UCCS - Unité de Catalyse et Chimie Du Solide, F-59000, Lille, France*

ARTICLE INFO

Keywords
Knoevenagel reaction
Push-pull dyes
Indane-1,3-dione derivative
Cyclization reaction
Azafluorenone

ABSTRACT

A series of twelve dyes have been designed using 2-(3-oxo-2,3-dihydro-1*H*-cyclopenta[*b*]naphthalen-1-ylidene)malononitrile as the electron acceptor. While using piperidine as a classical base for the Knoevenagel reaction, a nucleophilic attack of the amine on the formed push-pull chromophore occurred, producing an azafluorenone derivative. By varying the amine, a series of azafluorenones could be obtained. By using an aldehyde of extended conjugation, a spontaneous aromatization following the cyclization reaction could also be demonstrated. The optical, electrochemical properties of the different dyes were examined. Theoretical calculations were also carried out to support the experimental results.

1. Introduction

During the past decades, a great deal of efforts has been devoted to design push-pull chromophores as these structures can find applications in numerous research fields ranging from Non-Linear Applications (NLO) [1–6] to Organic Photovoltaics (OPVs) [7–12], Organic Fields Effects Transistors (OFETs) [13], Organic Light-Emitting Diodes (OLEDs) [14] and photoinitiators of polymerization [15–19]. Typically, a push-pull compound is composed of an electron donor connected to an electron acceptor by mean of a conjugated or a non-conjugated spacer but dyes comprising a conjugated spacer are the most popular ones. Among all possible reactions to create a π-conjugated linker, the Knoevenagel reaction consisting in the dehydrative condensation of an aldehyde with an activated methylene group is a reaction of choice for the preparation of push-pull structures and this reaction is most generally carried out under basic conditions. However, when strong electron acceptors are used, their anionic forms are stable under basic conditions, rendering these conditions ineffective to prepare push-pull dyes. In this case, use of acidic conditions are thus required, as exemplified with Knoevenagel reactions carried out in acetic anhydride. When basic conditions are employed, piperidine is without contest one of the most popular bases due to its relatively high pKa (11.1, 25 °C) which is sufficient to deprotonate activated methylene groups, its low cost, its low toxicity and easiness to evaporate [20]. However, to prepare dyes, the selection of the reaction conditions is of crucial importance as the amine can further react with the newly prepared dye, giving rise to the formation of side-products. This drawback is notably observed for all dyes prepared with 2-(3-oxo-2,3-dihydro-1*H*-inden-1-ylidene) malononitrile as the electron acceptors or its derivatives. A nucleophilic attack of the amine onto the dicyanomethylidene groups of the electron acceptor is occasionally observed. As a result of this, 3-(dialkylamino)-1,2-dihydro-9-oxo-9*H*-indeno [2,1-*c*] pyridine-4-carbonitrile derivatives can be obtained (See Fig. 1) [21]. Reaction yields ranging from 17 to 51% were obtained upon mixing one equivalent of aldehyde with one equivalent of base and one equivalent of electron acceptor at room temperature for 14 h.

In 2014, a better reaction yield was reported for the synthesis of **C5**, reaching 96%, by opposing one equivalent of diethylamine to the preformed push-pull dye 2-(2-(furan-2-ylmethylene)-3-oxo-2,3-dihydro-1*H*-inden-1-ylidene)malononitrile for 30 min at room temperature (see Fig. 2) [22]. This unexpected nucleophilic attack on the dicyanomethylidene group was notably observed during the synthesis of a series of photochromes based on Donor–Acceptor Stenhouse Adducts (DASA) [22]. More recently, a fluorescent probe for live cell imaging was developed with a triphenylamine using a similar approach and **C6** could be obtained in 47% yield after heating for 12 h at 50 °C [23].

* Corresponding author.
** Corresponding author.
E-mail addresses: corentin.pigot@univ-amu.fr (C. Pigot); frederic.dumur@univ-amu.fr (F. Dumur)

https://doi.org/10.1016/j.dyepig.2020.108182
Received 27 September 2019; Received in revised form 29 November 2019; Accepted 1 January 2020
Available online xxx
0143-7208/

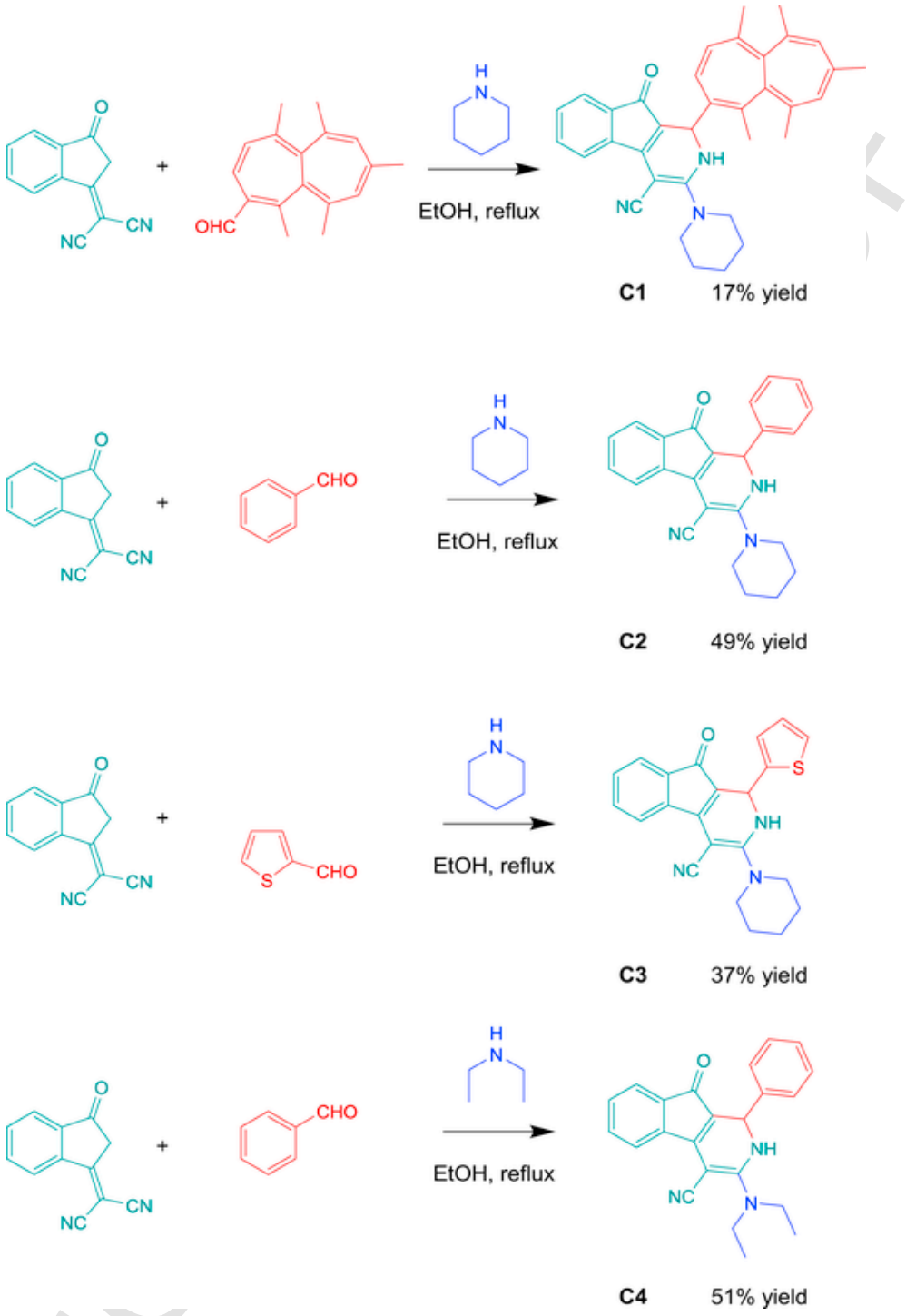

Fig. 1. Chemical structures of 3-(dialkylamino)-1,2-dihydro-9-oxo-9*H*-indeno[2,1-*c*]pyridine-4-carbonitrile derivatives **C1–C4** formed by nucleophilic attack of the amine catalysts.

From these different works, it can be concluded that the formation of the push-pull compound arises prior the nucleophilic attack of the amine onto the dicyanomethylidene group and therefore the cyclization reaction.

Also, the following mechanism was proposed to support the formation of 3-(dialkylamino)-1,2-dihydro-9-oxo-9*H*-indeno [2,1-*c*]pyridine-4-carbonitrile derivatives (See Fig. 3).

In this work, we report on the synthesis of two new push-pull dyes **PP1** and **PP2** based on 2-(3-oxo-2,3-dihydro-1*H*-cyclopenta[*b*]naphthalen-1-ylidene)malononitrile **EA1** as the electron acceptor. To date, **EA1** has only been scarcely used to prepare dyes [24–26] despite its promising electron-withdrawing ability. We also drastically optimized the synthesis of 1*H*-cyclopenta[*b*]naphthalene-1,3(2*H*)-dione **EA2** so that this precursor of **EA1** could be obtained with reaction yields higher than 90%. To evaluate the benefit of **EA1** in the optical properties of **PP1** and **PP2**, their analogues **PP3** [27] and **PP4** [28] using 2-(3-oxo-2,3-dihydro-1*H*-inden-1-ylidene)malononitrile as the acceptor were prepared and the optical properties compared to those of **PP1** and **PP2** (see Fig. 4). It has to be noticed that the synthesis of these two dyes (**PP3** and **PP4**) has been previously reported in the literature. Par-

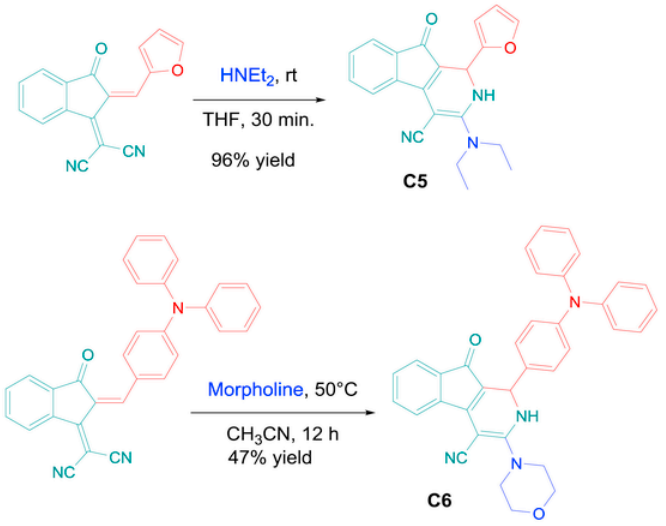

Fig. 2. Chemical structure of **C5** prepared from 2-(2-(furan-2-ylmethylene)-3-oxo-2,3-dihydro-1*H*-inden-1-ylidene)malononitrile and structure of **C6.**

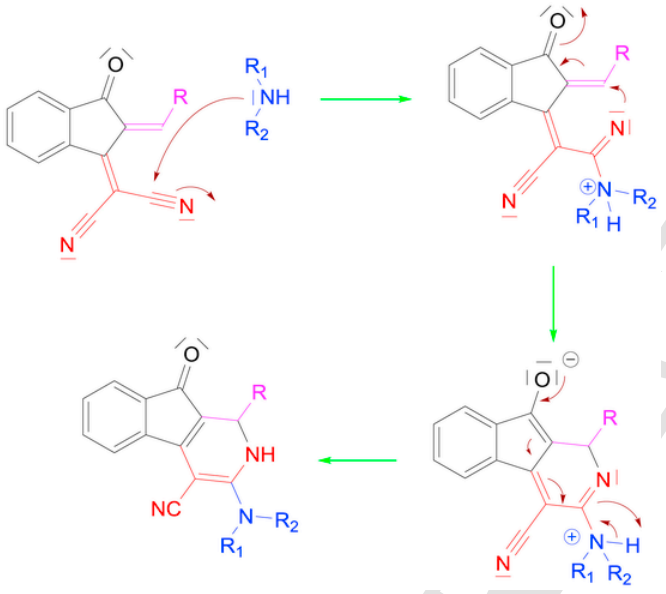

Fig. 3. Mechanism resulting in the synthesis of 3-(dialkylamino)-1,2-dihydro-9-oxo-9*H*-indeno [2,1-*c*]pyridine-4-carbonitrile derivatives.

allel to this, during the course of our investigations, choice of the amine used for the Knoevenagel reaction was determined as being crucial to avoid the nucleophilic attack of this latter on the push-pull structures so that a series of amines were tested as catalysts. The different products obtained during these different reactions and their properties are also reported and discussed.

2. Results and discussion

2.1. 1- Synthesis of the different compounds

As mentioned in the introduction section, the first step consisted in preparing **EA1** starting from **EA2**. Compared to previous reports [29,30], the reaction yield to get **EA2** was greatly improved, based on several modifications. Notably, a typical procedure to access to **EA2** consists in a Claisen reaction of a dialkyl naphthalene-2,3-dicarboxylate with ethyl acetate in the presence of a base (See Fig. 5).

By increasing the quantity of sodium hydride (2.5 eq. instead of 1.45 eq.) for the first step and by elongating the decarboxylation time (1h30 instead of 20 min) for the second step, the reaction yield could be increased up to 91%, higher than the 65% yield reported in the literature. Noticeably, safer conditions were used for the recrystallization step of **EA2**, in which benzene was replaced by toluene. Finally, the functionalization of **EA2** by malononitrile was carried out under standard conditions, using sodium acetate as the base. **EA1** could be obtained in 67% yield, as previously described in the literature [31]. After the preparation of **EA1**, the synthesis of the different push-pull dyes described in Fig. 4 were realized, starting with **PP1**. This synthesis consisted in a Knoevenagel reaction between **EA1** and 4-*N,N*-dimethylaminobenzaldehyde **ED1** in the presence of a base, currently piperidine, in ethanol for 30 min.

Unexpectedly, the reaction media turned red and the structure of a new compound, **PP6**, was confirmed by NMR spectroscopy (See Fig. 6). Nevertheless, this reactivity of secondary amines, like piperidine, has already been highlighted in the literature, in 2008, by Landmesser et al. [21]. As no such reaction has been previously described concerning α,β-unsaturated aldehydes, the same procedure was used for **PP2**, using the same conditions. After 30 min of reaction, if the Nuclear Magnetic Resonance (NMR) analyses confirmed the absence of the targeted chromophore **PP2** in the reaction media, a red colour was also observed for this second reaction opposing **EA1** to **ED2** (See Fig. 6).

Surprisingly, analyses by ^{1}H NMR spectroscopy in $CDCl_3$ revealed the electron-donating moiety **ED2** not to be connected to **EA1**. On the opposite and unexpectedly, the covalent linkage of piperidine to **EA1** could be easily evidenced by ^{1}H NMR analyses, with the presence of two sets of signals at 1.85 and 3.86 ppm. Presence of a singlet at 5.87 ppm integrating for one proton could also be detected. Finally, the exact structure of **PP5** could be revealed by X-ray diffraction (see Fig. 7).

The single crystals of **PP5** suitable for X-ray crystallographic analyses were grown by slow evaporation of $CDCl_3$ solvent in the NMR tube. The detailed crystallographic data are given in the Electronic Supporting Information.

As evidenced in Fig. 8, the mechanism inducing the formation of **PP5** results from the nucleophilic attack of piperidine on the polarized ketone group. After prototropy, a dehydration reaction resulting from the deprotonation of the activated methylene group by piperidine can occur, providing **PP5** as a red powder. Interestingly, attempts to prepare **PP5** by simply refluxing **EA1** in ethanol, in the presence of piperidine failed to produce **PP5** and only traces of product were detected by thin layer chromatography (TLC) even after 2 h of reflux (See Fig. 6). Upon addition of **ED2**, immediately, the reaction colour turned deep red and a complete consumption of **EA1** was observed within 20 min. If the exact role of **ED2** is not fully understood, **ED2** clearly favours the synthesis of **PP5**. It can be tentatively assigned to a role of base, this electron donor comprising a dimethylaniline moiety probably facilitating the deprotonation occurring in last step.

Considering that **PP6** was also obtained as a red solid, that its absorption properties are clearly centered in the visible range with a small Highest Occupied Molecular Orbital (HOMO)-Lowest Unoccupied Molecular Orbital (LUMO) gap [21], the design and synthesis of a series of dyes still based on **EA1** as the electron acceptor but differing by the electron-donating groups and the amine pendant groups were realized. The first parameter investigated was the influence of the amine on the reaction yields and the optical properties of the resulting products while keeping **ED1** as the electron donor. In this aim, five different amines were investigated. Secondly, the influence of the conjugation length between the electron-donating part and the electron-withdrawing group on both the reaction yields and the optical properties was examined. For this purpose, another electron donor, namely **ED2** was used (See Fig. 10). A summary of the different product obtained during these syntheses and the corresponding reaction yields are provided in Table 1. Even if no clear conclusion can be made concerning the im-

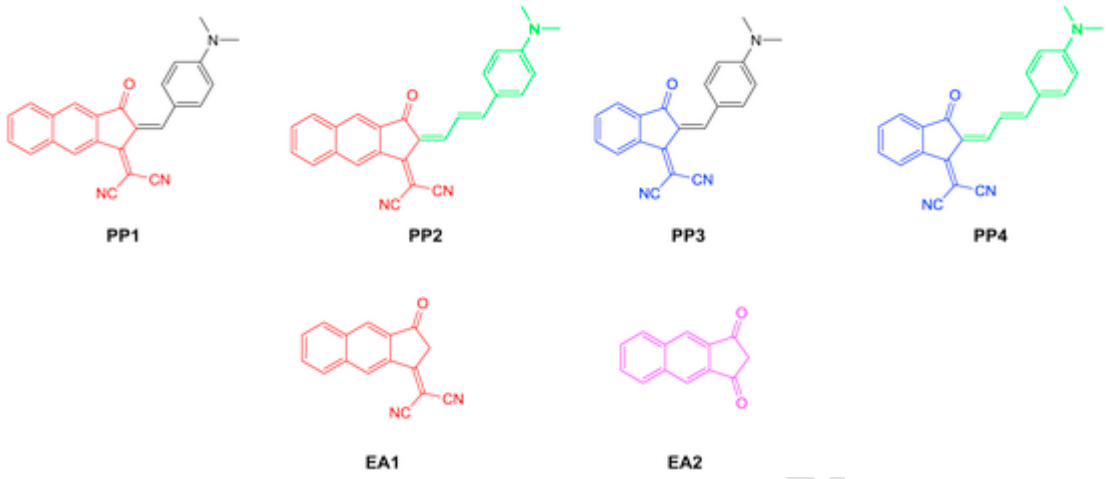

Fig. 4. Chemical structures of push-pull dyes **PP1** and **PP2**, their analogues **PP3** and **PP4** and the electron acceptors **EA1** and **EA2**.

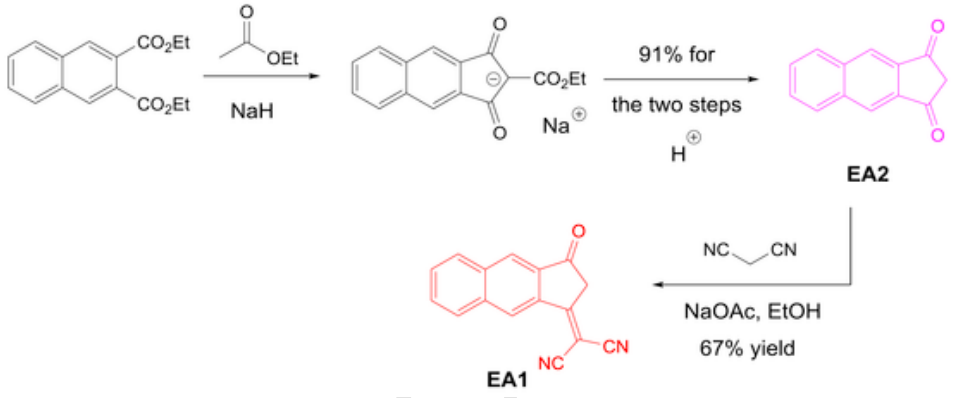

Fig. 5. Synthetic routes to **EA1** and **EA2**.

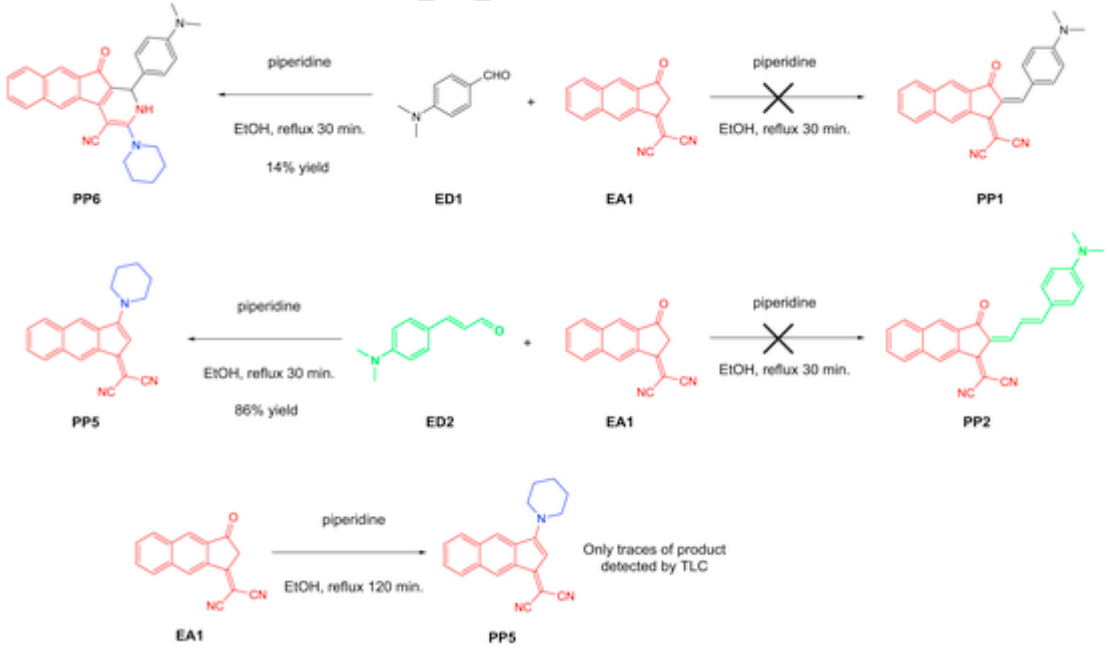

Fig. 6. Synthetic route to the targeted **PP1** and **PP2** dyes, and chemical structures of the unexpected **PP5** and **PP6** adducts formed using piperidine as the base.

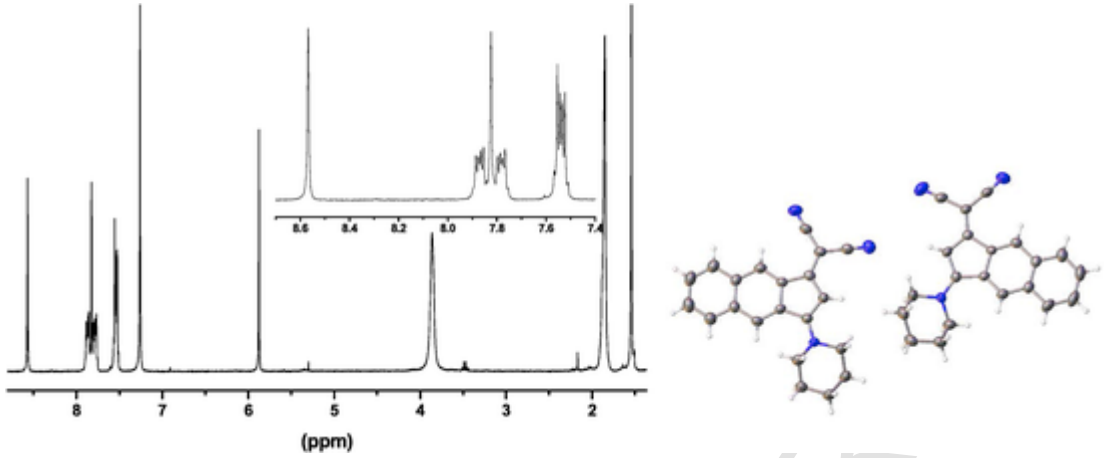

Fig. 7. ^{1}H NMR spectrum of **PP5** done in $CDCl_3$ (7.26 ppm) (left) and crystal structure of **PP5** (right).

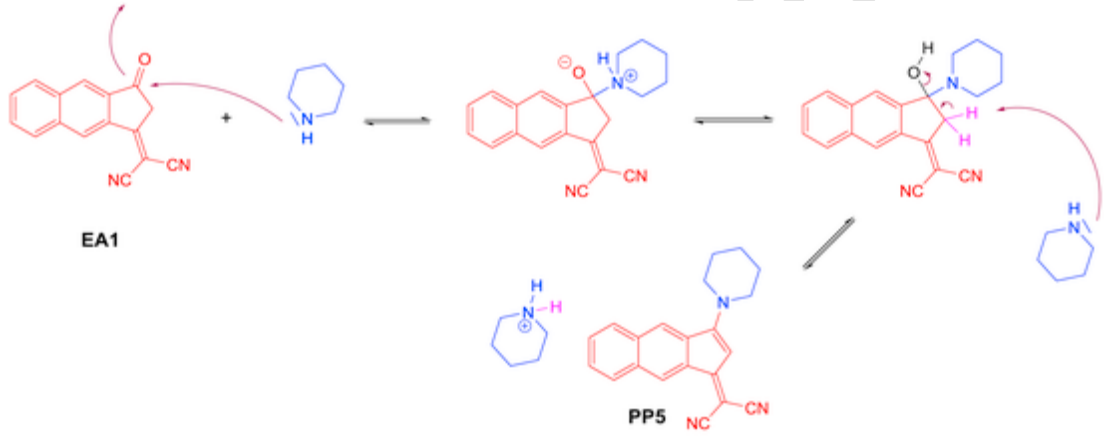

Fig. 8. Mechanism inducing the formation of **PP5**.

Table 1
Isolated yields obtained with different amines during the synthesis of azafluorenones using **ED1** or **ED2** as the donors.

Amine	ED1	ED2
	**PP6** (14%)	**PP5** (86%)
	**PP7** (79%)	**PP11** (6%)
	**PP8** (35%)	**PP12** (18%)
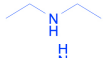	**PP9** (10%)	**PP13** (5%)
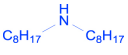	**PP10** (5%) + **PP10'** (25%)	**PP2** (60%)

pact of the basicity of the amine on this reaction, we clearly demonstrate that higher reaction yields were obtained when cyclic aliphatic amines were used during the synthesis of **PP6-PP10** (See Fig. 9). It might be explained by the higher availability of the nitrogen lone pair electrons in this case. In fact, the cycle drastically inhibits the pyramidal inversion of the nitrogen atom.

Concerning the disparity of the reaction yields, two factors might also be considered. Firstly, for morpholine and pyrrolidine, no column chromatography was necessary to get the product in pure form, the dyes directly precipitating by addition of acetone to the reaction media. In these conditions, the products could be obtained in high yields. As further detailed in the NMR section, a facile protonation of the dihydro-2-azafluorenes in chloroform was clearly evidenced, resulting in the duplication of the NMR signals (see ^{1}H NMR spectra in SI).

Considering that $CDCl_3$ is sufficiently acidic to protonate the dyes in solution, it also means that during the purification process, a non-negligible part of the products was lost by adsorption onto the stationary phase (silicagel), chloroform being used as the eluent. Therefore, it may also explain why **PP9** or **PP10** were isolated in pure form only in low yields. The formation of the aromatized product observed in the case of **PP10** and producing **PP10'** also contributes to reduce the final reaction yield. To confirm the chemical structure of these dihydro-2-azafluorenes, crystals could notably be obtained upon slow evaporation of chloroform. The crystal structure of **PP10** in presented in Fig. 9.

Regarding the condensation of **ED2** onto **EA1** and the subsequent nucleophilic attack of the amine, adducts totally differing in structures from that obtained with **ED1** were obtained, evidencing a significant difference of reactivity with the elongated aldehyde **ED2**. Notably, a spontaneous aromatization resulting in the formation of a pyridine group was notably evidenced with **PP11**, **PP12** and **PP13** (See Fig. 10). The crystal structure of **PP12** is presented in Fig. 10.

Elongation of the π-conjugation therefore favoured the oxidation (and the aromatization process), providing the pyridine adducts **PP11**, **PP12** and **PP13** as the main products of a one-pot synthesis. Formation of such aromatized structures has been previously reported by Landmesser et al. [21] While using aldehydes of short conjugation length, by developing a two-step procedure where chemical oxidants

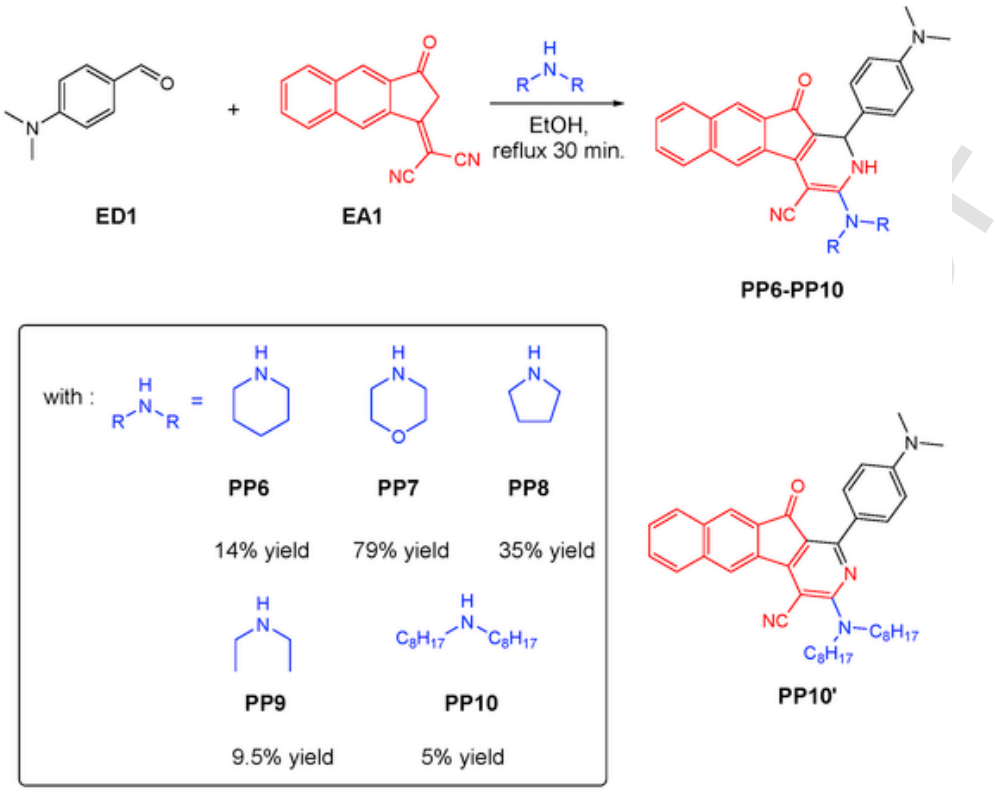

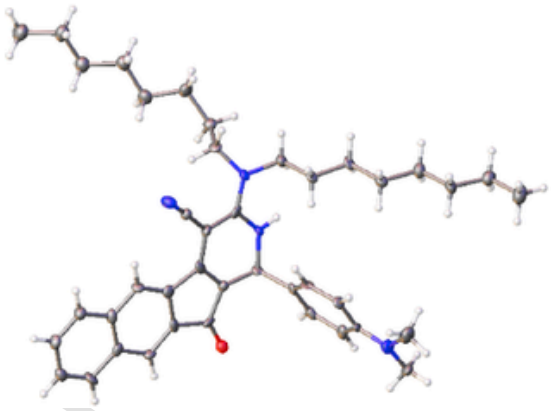

Fig. 9. Synthetic route to **PP6-PP10** and crystal structure of **PP10**.

($KMnO_4$, chloranil) were used, the access to aromatized structures was possible. Besides, it has to be noticed that Landmesser et al. also detected the coexistence of the aromatized and none-aromatized forms during the course of their investigations, but the aromatized products were only detected as a minor side-product of the reaction. Surprisingly, while using dioctylamine as the amine, the cyclization product was not detected in the reaction media. Instead, **PP2** could be isolated in pure form in 60% yield, demonstrating either a steric hindrance of the amine or a better kinetic favouring the Knoevenagel reaction. After investigating the synthesis of the different azafluorenones **PP6-PP13**, we focused our work on the synthesis of the initially desired push-pull dyes **PP1** and **PP2** and their analogues **PP3** and **PP4** (see Fig. 11).

As previously evidenced, it appeared that the main drawback encountered with piperidine was its nucleophilicity. To overcome this drawback, a none-nucleophilic base was selected for the Knoevenagel reactions, namely *N,N*-diisopropylethylamine (DIPEA). Indeed, the steric hindrance of this tertiary amine prevents its nucleophilic addition onto **PP1-PP4**. As expected, **PP1-PP4** were obtained with reaction yields ranging between 55 and 65% (See Fig. 11). Formation of these products were confirmed by ^{1}H and ^{13}C NMR analyses.

Finally, after the successful synthesis of **PP1-PP4** by using DIPEA as the base, the possibility to convert these push-pull structures into azafluorenones was examined. As a proof of concept, the conversion of **PP1** to **PP6** and **PP2** to **PP12** was examined. In the two cases, slightly higher reaction yields were obtained compared to the direct one-pot synthesis, resulting from the fact that the push-pull dyes **PP1** and **PP2** are already formed and purified prior to the cyclization reaction occurring in final step. (See Fig. 12).

3. 2- ^{1}H NMR spectroscopy study

As above-mentioned in the text, the different cyclization products proved to be highly sensitive to the protic character of the solvent. This point was notably evidenced by the low isolated reaction yields obtained for the different compounds after chromatographic purification.

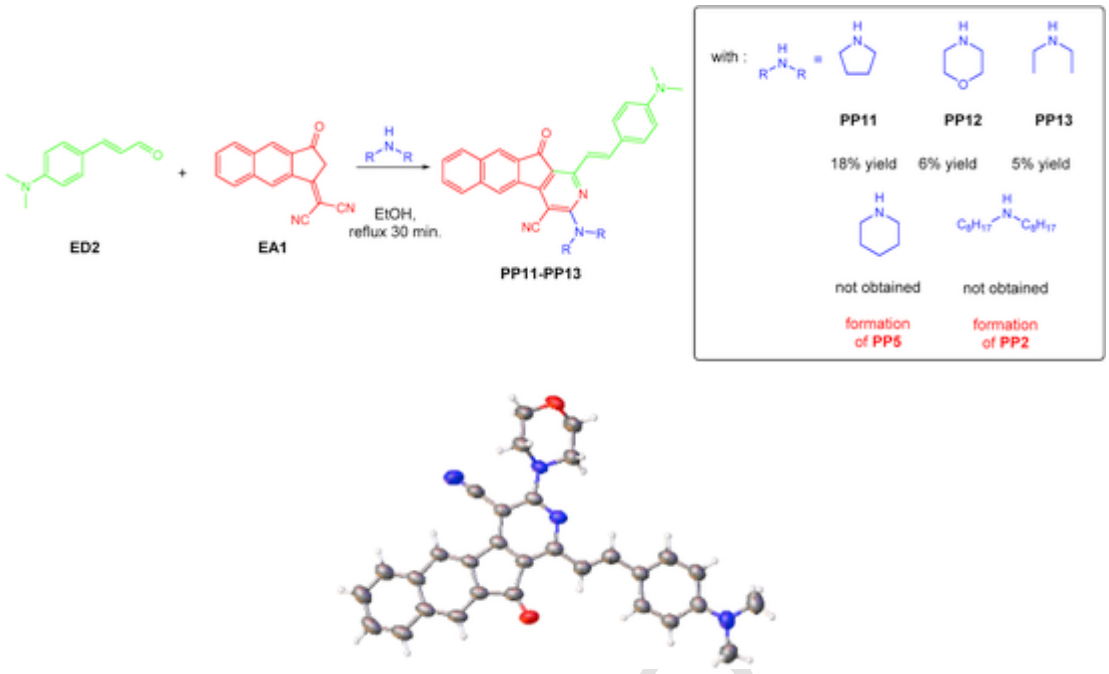

Fig. 10. Synthetic route to **PP11-PP13** and crystal structure of **PP12**.

This also explains that most of the product remaining immobilized on the acidic silica gel during the complex separation of numerous products by column chromatography. Face to this consideration, this point was also explored by NMR spectroscopy. Two different solvents enabling to perfectly solubilize the different compounds (**PP6**, **PP7**, **PP8, PP9** and **PP10**) were tested, namely, a protic solvent i.e. chloroform and an aprotic one i.e. DMSO. Fig. 13 displays the NMR data of **PP8** in the two selected solvents.

If a clear ^{1}H NMR spectrum corresponding to the targeted molecule was obtained in DMSO-d_6, the coexistence of two different forms could be found in the ^{1}H NMR spectrum of **PP8** in deuterated chloroform (see Fig. 13). Indeed, the protonated and the none-protonated form could be determined as being in a 31:69 ratio, the none-protonated state constituting the main form in the sample. Examination of the behaviour of these five chromophores in the two solvents revealed **PP7**, **PP8**, and **PP9** to be the most sensitive compounds of the series, ratios of 21:79 and 28:72 being respectively determined for **PP7** and **PP9**. As specificity for **PP7**, traces of the protonated form could be even detected in DMSO, evidencing its easy protonation (See ^{1}H NMR spectra in SI). Conversely, **PP6** proved to be insensitive to the acidic character of chloroform, no trace of protonation being detected by NMR. It has to be noticed that all cyclization reactions have been carried out in the presence of an excess of base so that the protonation detected by ^{1}H NMR can only originate from acidic traces in the deuterated solvents.

3.1. 3-UV-visible absorption and photoluminescence spectroscopy

All compounds reported in this work are stable under air, even when diluted in solution so that photophysical measurements could be carried out. As evidenced by NMR analyses, if a protonation for some of the dyes in protic solvents could be demonstrated, no photodegradation of the dyes were detected by NMR during the course of our investigations. Especially, no modification of the NMR signals was detected even for NMR tubes exposed to sunlight during several weeks. In this context, the dyes being stable in solution, these latter could be characterized by UV–visible absorption spectroscopy and the different absorption spectra were recorded in three different solvents, namely chloroform, dichloromethane and DMSO. Interestingly, four different but characteristic UV–visible spectra were found for the cyclized compounds, depending of the length of the conjugated spacer between the electron-donating dimethylaminophenyl group and the electron-accepting azafluorenone moiety, but also to the fact that the pyridine group of the azafluorenone moiety is aromatized or not. Thus, the UV/Vis absorption spectra of the dihydro-2-azafluorenones **PP6**, **PP7**, **PP8**, **PP9**, and **PP10** are dominated by an intensive intramolecular charge-transfer (ICT) band extending between 440 and 600 nm irrespective of the solvent (See Fig. 14).

By changing the appended amine, no shift of the ICT band was found for all compounds, evidencing the push-pull effect to be independent of this substituent. The lack of contribution on the push-pull effect were confirmed by theoretical calculations. As illustrated in Fig. 15 and the corresponding Figures in SI, only the nitrogen atom of the pendant amine was determined as contributing to the highest Occupied Molecular Orbital (HOMO) and the Lowest Unoccupied Molecular Orbital (LUMO). No extension over the alkyl chain of the different amines (piperidine, morpholine, dioctylamine, diethylamine or pyrrolidine) was found, justifying the dihydro-2-azafluorenones to be insensitive to this substitution pattern. For all dyes, an absorption maximum peaking at 500 nm was determined for the five chromophores **PP6-PP10** and in the three different solvents. A HOMO-LUMO gap of 2.48 eV was calculated for all dyes. Comparison of the experimental absorption spectra with those determined by theoretical calculations revealed the absorption maxima to be red-shifted by about 13 nm relative to that determined theoretically, this latter peaking at 487 nm.

Besides, a good agreement between the experimental and the theoretical values are thus found for the absorption maxima. Apart from the ICT band, three absorption peaks could also be detected between 350 and 430 nm and origins of these transitions were assigned to HOMO-5/-4/-3 → LUMO transitions admixed with HOMO-1 → LUMO + 1, HOMO → LUMO + 1 transitions (See Table 2).

Finally, the intense high-energy bands in the 300–350 nm region typically correspond to localized aromatic π-π* transitions of the chromophores. Examination of their UV–visible absorption properties in chloroform revealed the absorption spectra of all dyes to be similar to those determined in DMSO or dichloromethane (See Fig. 14), despites the partial protonation of the dihydro-2-azafluorenones in chloroform.

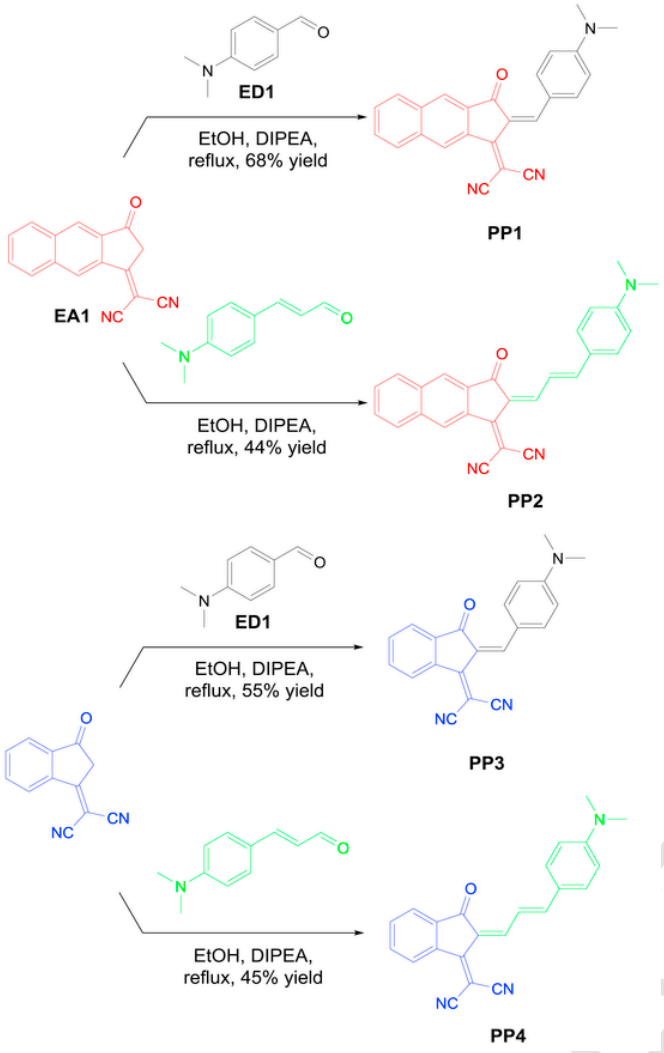

Fig. 11. Synthetic route to **PP1-PP4**.

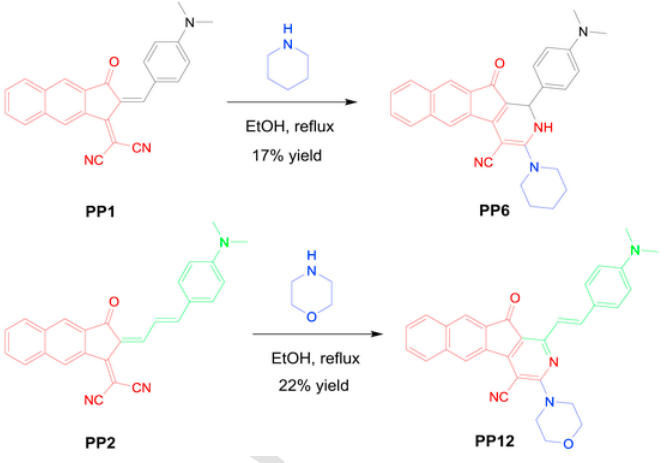

Fig. 12. Synthetic route to **PP6** and **PP12** starting from **PP1** and **PP2**.

Unexpectedly, elongation of the spacer between the electron donor and the electron acceptor in **PP11**, **PP12** and **PP13** resulted in a hypsochromic shift of the absorption maxima irrespective of the amine substituents. Indeed, absorption maxima peaking at 480 nm was found for the three dyes, blue-shifted by about 20 nm relative to the previous series. Here again, absence of contribution of the amino group to the push-pull effect was evidenced, the three absorption spectra superimposing each other. Conversely and as anticipated, elongation of the spacer resulted in a significant increase of the molar extinction coefficients of the ICT bands for **PP11**, **PP12** and **PP13** relative to those of the previous dihydro-2-azafluorenones (**PP6-PP10**), resulting from an enhancement of the oscillator strength. Here again, comparison of the theoretical and experimental absorption spectra revealed a good agreement between both. Two main transitions were detected in DMSO, in the 350–420 nm and 420–600 nm regions, the second one corresponding to the ICT band of the chromophores. Positions of these transitions are close to those determined theoretically, the simulated spectra displaying two main absorption bands at comparable positions (See Fig. 16).

A difference as small as 14 nm were found between the theoretical (492 nm) and the experimental (478 nm) absorption maxima. Comparison of the theoretical calculations carried out on the dihydro-2-azafluorenones and the 2-azafluorenones revealed the HOMO energy level of dihydro-2-azafluorenones to benefit from both the electron-donating effects of the dimethylaminophenyl group and the amino pendant group. Conversely, as evidenced in Fig. 17, only the dimethylaminophenyl group of 2-azafluorenones contributes as the electron donor, supporting the blue-shift detected for the ICT bands.

Upon aromatization, a clear modification of the absorption spectra could be evidenced between the dihydro-2-azafluorenone **PP10** and the 2-azafluorenone **PP10′** corresponding to the aromatized version of **PP10**. As shown in Fig. 18, a blue-shift of the ICT band was observed upon aromatization of the pyridine moiety, the absorption maximum shifting from 500 nm for **PP10** to 430 nm for **PP10'**. These results are consistent with a reduced electronic delocalization upon aromatization, what is notably observed when quinones are converted to hydroquinone derivatives [32]. Parallel to this, the two intense high-energy bands in the 300–350 nm region detected for **PP10** were not visible anymore in the absorption spectrum of **PP10'**. While using the same theoretical model, only a slight shift of the ICT band is observed upon aromatization. Notably, absorption maxima peaking at 481 and 448 nm are theoretically determined for **PP10** and **PP10′** respectively. If a good accordance is found between the experimental and the theoretical absorption maximum for **PP10** (496 nm and 482 nm respectively) and **PP10'** (434 and 447 nm respectively), a complete mismatch between the theoretical and experimental molar extinction coefficients was found. This is attributable to the long alkyl chains that rendered the optimization of structures and the subsequent calculations difficult to be carried out (see Fig. 19).

Finally, the most intriguing absorption spectrum was obtained for **PP5**, resulting from the nucleophilic addition of piperidine on the electron acceptor **EA1**. Presence of numerous optical transitions could be found between 300 and 600 nm irrespective of the solvent, making this dye a panchromatic chromophore (see Fig. 18). Based on the theoretical calculations, a few transitions could be assigned. Notably, in the 300–380 nm region, the different transitions can be assigned to an admixture of HOMO-1→LUMO + 1 and HOMO-2 → LUMO transitions. Conversely, in the 380–440 nm region, the absorption band is dominated by the HOMO-1→LUMO and HOMO→LUMO + 1 transitions. At low energy, a broad peak composed of multiple transitions extending from 450 nm to 600 nm and dominated by the HOMO→LUMO transition was found. An absorption maximum peaking at 506 nm was found for **PP5**, close to that obtained for the dihydro-2-azafluorenones **PP6-PP10** (500 nm).

It must be noticed that the complexity of the transitions detected by absorption spectroscopy can be tentatively assigned to the coexistence of two forms in solution, the neutral form and its corresponding zwitterion, complexifying the absorption spectrum. By examining the UV spectra of **PP1-PP4** in chloroform (see Fig. 20), several trends can be

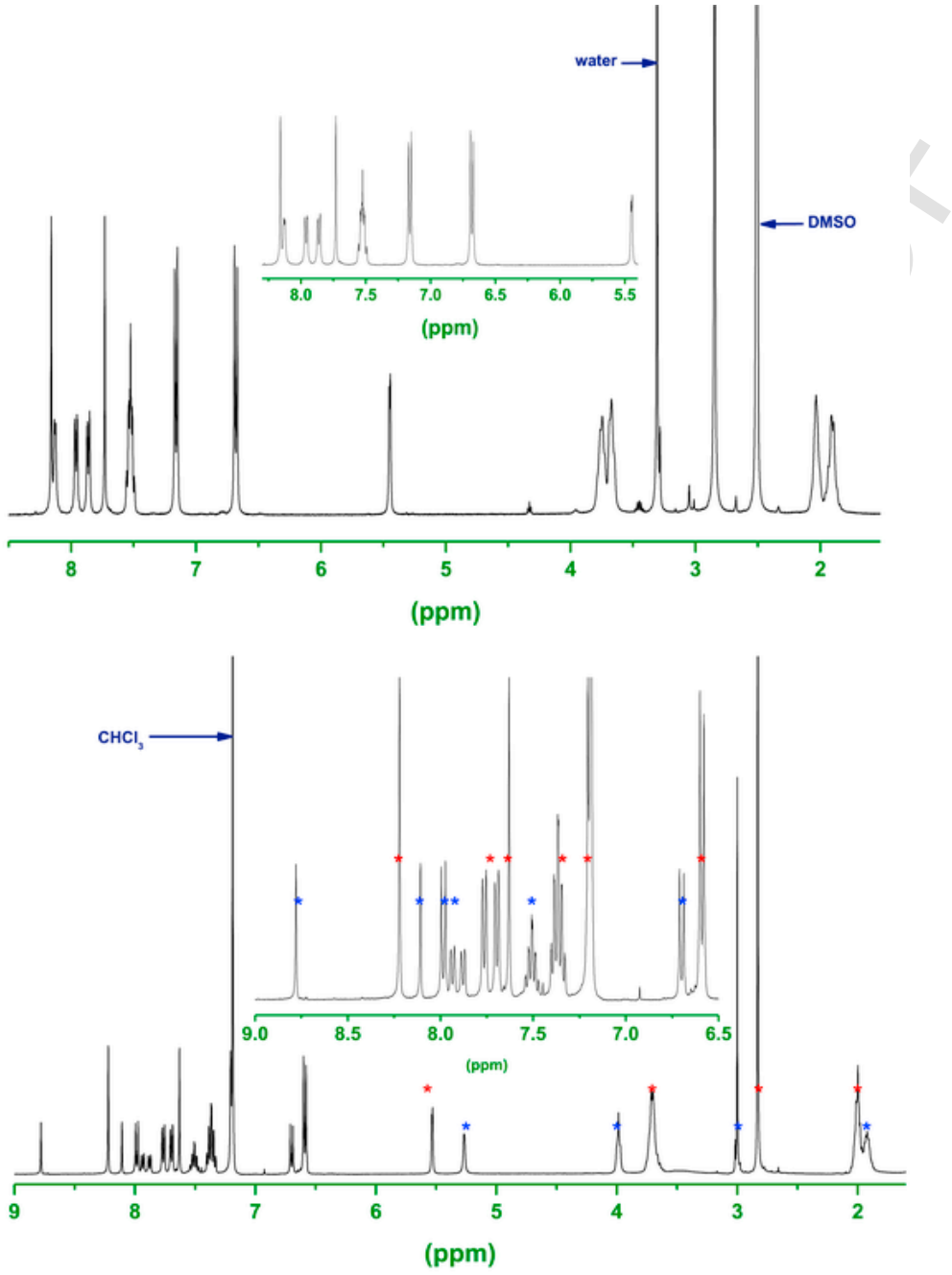

Fig. 13. Top: ^{1}H NMR spectra of **PP8** in DMSO-d_6. Bottom: ^{1}H NMR spectra of **PP8** in $CDCl_3$ with the protonated form representing 31% of the sample. (stars indicate the NMR signals corresponding to the product (*) and its protonated form (*).

deduced. As described at the beginning of the study, influence of two factors are studied in this paper, namely the impact of the additional phenyl ring on the electron-withdrawing ability of **EA1** and the role of the conjugated spacer on the optical properties of **PP1-PP4**. Concerning the elongation of the aromatic scaffold of **EA1**, a red-shift absorption by about 30 nm is observed while comparing **PP1** and **PP3, PP2** and **PP4** i.e. at similar electron-donating group and spacer (see Fig. 20). It can be thus concluded that a stabilization of the LUMO energy level is observed for **EA1** compared to its analogue 2-(3-oxo-2,3-dihydro-1*H*-inden-1-ylidene) malononitrile. Concerning the extension of the π-conjugation of the spacer in **PP2** and **PP4**, an even bigger red-shift of 80 nm is detected. As previously reported in the literature, the HOMO of push-pull structure comprises both the electron-donating group and the π-conjugated spacer [33]. Upon elongation of the spacer, a destabilization of the HOMO level occurs, resulting in a decrease of the HOMO-LUMO gap and a red-shift of the absorption spectrum towards long wavelengths. Theoretical calculations carried out on **PP1-PP4** confirmed the order determined in solution (See Fig. 20) and the distribution of the electronic density on the HOMO and LUMO energy levels (See Fig. 21).

Finally, the emission properties of all dyes were examined in dichloromethane as the solvent. Here again, each series displayed a typical fluorescence spectrum, with an emission centered in the visible range (See Fig. 22). Thus, for the dihydro-2-azafluorenones **PP6**-**PP10**, an emission peaking between 568 and 570 nm could be determined. The emission peaks for **PP11**-**PP13** were found at 574 nm, close to that

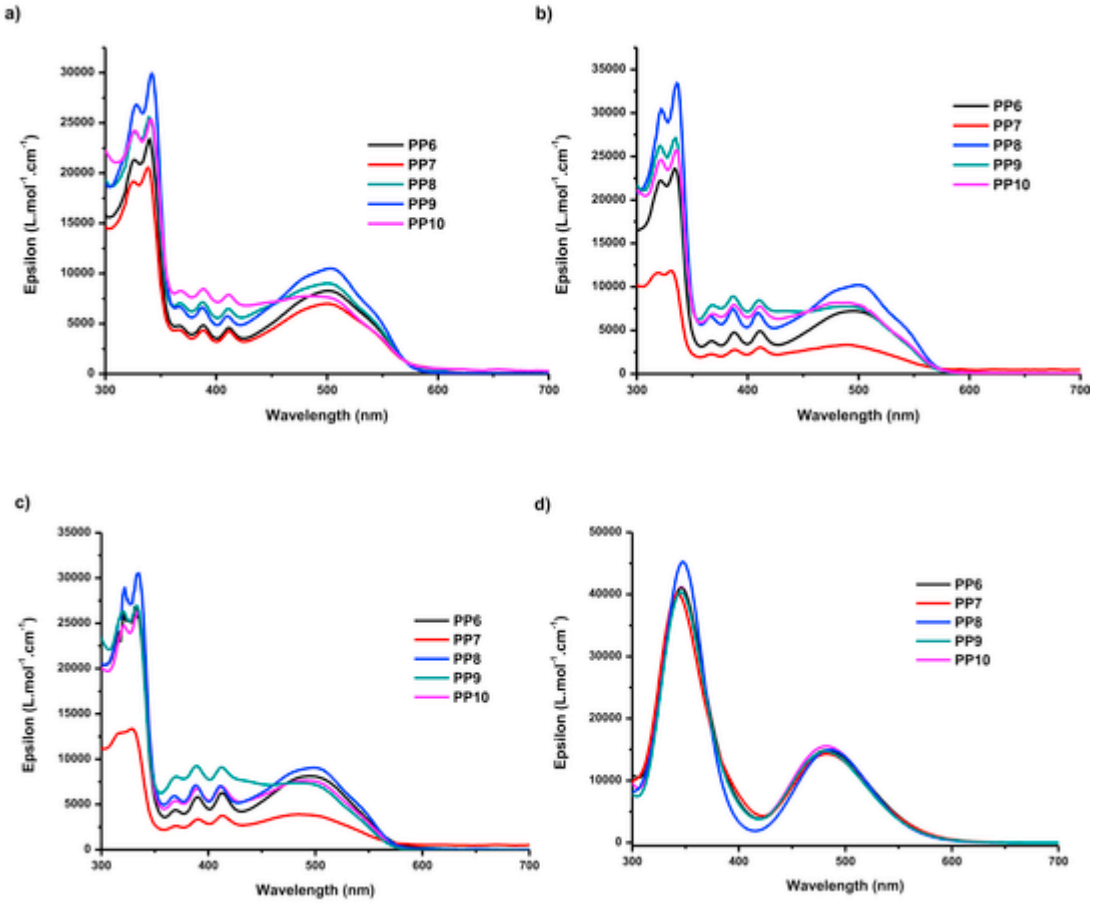

Fig. 14. UV–visible absorption spectra of dihydro-2-azafluorenones **PP6-PP10** in DMSO (a), dichloromethane (b), chloroform (c) and the theoretical UV–visible absorption spectra in dichloromethane (d).

obtained for the former series despites the presence of the elongation of the conjugated spacer introduced between the donor and the acceptor. Upon aromatization of dihydro-2-azafluorenones, no significant change was found in the PL spectrum of **PP10**', displayed an emission maximum superimposing that of the two previous series. Therefore, it can be concluded that the energetic transition involved in these different dyes are similar. Interestingly, **PP5** that drastically differs from the others by the absence of the dimethylaminophenyl group could emit at 562 nm. Stokes shift values of 70 and 95 nm were determined for the dihydro-2-azafluorenones **PP6-PP10** and the 2-azafluorenones **PP11-PP13** respectively. It can be therefore concluded that a higher electronic redistribution occurs upon excitation of the 2-azafluorenones relative to the dihydro-2-azafluorenones.

3.2. 4-Cyclic voltammetry

The electrochemical properties of all compounds have been investigated by cyclic voltammetry (CV) in a dilute solution of dichloromethane. All solutions have been deaerated with argon for 10 min prior to CV measurements. Besides this, traces of oxygen could be still detected on certain CV spectra, attributable to a strong interaction between dyes and oxygen. In this context, determination of the reduction potentials for several dyes was affected by the presence of oxygen, underestimating the real energy level of the LUMO orbitals. The redox potentials of the compounds **PP1-PP13** are summarized in Table 3 in which the redox potentials are given against the half wave oxidation potential of the ferrocene/ferrocenium cation couple. The values of the HOMO and LUMO energy levels of the different chromophores were also determined using as the standard the value of the oxidation potential of ferrocene (Fc) based on the calculations of Pommerehne et al. (4.8 eV vs. vacuum) [34]. The obtained values of E_{HOMO} and E_{LUMO} are summarized in Table 3. Fig. 23 allows a comparison of the redox potentials of **PP1-PP4** molecules. Notably, **PP1** and **PP2** possess the same electron acceptor and the oxidation potentials vary with the contribution of the electron-donating part that includes the electron donor for **PP1**, but also the conjugated spacer in the case of **PP2**.

As a result of this, elongation of the conjugated spacer facilitates the oxidation process in **PP2** relative to **PP1** and a decrease of the oxidation potential of 250 mV was observed (See Fig. 23a). Parallel to this, a modification of the reduction process centered onto **EA1** was also detected, a cathodic shift of 150 mV being evidenced for the reduction peak of **PP2** relative to **PP1**. This cathodic shift of the reduction peak upon elongation of the π-conjugated spacer is quite unusual, considering that the same electron acceptor is present in the two molecules. To support this shift, repartition of the respective HOMO and LUMO energy levels of **PP1** and **PP2** have to be considered. As shown in Fig. 21, the HOMO levels of **PP1** and **PP2** is mainly centered onto the electron-donating group with a contribution of the spacer. Conversely, the LUMO levels extend over the whole molecule. As a result of this, and due to the contribution of the electron-rich electron donating group to the LUMO level, a reduced electron-withdrawing ability is observed for **PP2**, shifting the reduction peak at lower potential than that of **PP1**. While comparing the dyes at identical electron donor, **EA1** proved to be a better electron acceptor than 2-(3-oxo-2,3-dihydro-1*H*-inden-1-ylidene)malononitrile, the irreversible reduction of the electron acceptor in **PP1** occurring at less cathodic potentials than for **PP3** (−1.27 V vs.

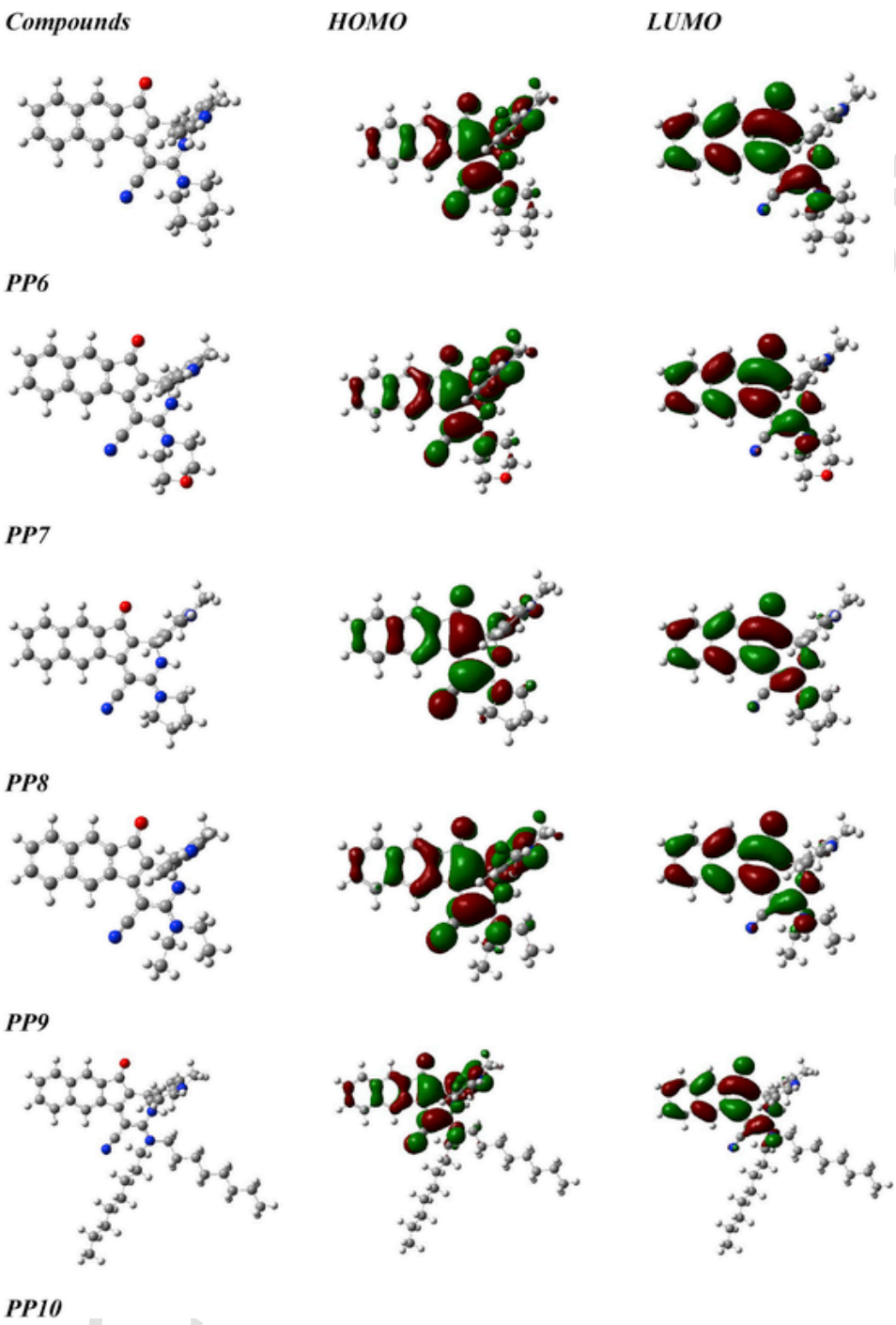

Fig. 15. Optimized geometries and contour plots of the HOMO and LUMO energy levels for the non-aromatized azafluorenones compounds (**PP6-PP10**).

−1.35 V). By electrochemistry, an experimental determination of both the HOMO and the LUMO energy levels can be done from the onset of the oxidation and the reduction peaks. An electrochemical bandgap can be thus determined. As shown in Table 3, a good accordance between the theoretical and the optical bandgaps of **PP1-PP4** can be found. On the opposite, the electrochemical bandgaps underestimate the values of approximately 0.5 eV for all dyes. A different behaviour was evidenced with **PP5** for which an irreversible oxidation and a reversible reduction process could be evidenced (See Fig. 23c). Considering that **PP5** is substituted by a piperidine group and that the oxidation process is centered on the nitrogen atom, an oxidation peak is logically detected at a higher potential than that observed for **PP1-PP4**, the oxidation of aliphatic amines being more difficult than for the aromatic ones.

Compared to **PP1-PP4**, reduction of **PP5** is detected at a more cathodic potential, attributable to the lower electron-withdrawing ability resulting from a LUMO energy level extending over the whole molecule and notably the electron-donating piperidine moiety. Fig. 23d presents the voltammograms of **PP8** and **PP9** which differ only by the nature of the pendant amine. As evidenced by theoretical calculations, only the nitrogen atom of the pendant amines contributes to the HOMO and LUMO energy levels (see Fig. 17). The oxidation processes for **PP8** and **PP9** are centered on the same fragments of the molecule so that the two compounds exhibit irreversible oxidation processes located at iden-

Table 2
Summary of simulated absorption characteristics in dilute dichloromethane of a selected set of synthetized compounds. Data were obtained in dichloromethane solution.

Compounds	E_{HOMO} (eV)	E_{LUMO} (eV)	λ_{max} (nm)	Transitions
PP5	−5.955	−2.914	477	HOMO- > LUMO (92%) HOMO-2- > LUMO (7%)
PP6	−5.392	−2.217	496	HOMO- > LUMO (95%)
PP7	−5.504	−2.320	496	HOMO- > LUMO (96%)
PP8	−5.283	−2.103	496	HOMO- > LUMO (89%) HOMO-1- > LUMO (9%)
PP9	−5.401	−2.211	496	HOMO- > LUMO (95%)
PP10	−5.367	−2.176	487	HOMO- > LUMO (92%)
PP11	−5.283	−2.379	496	HOMO- > LUMO (95%)
PP12	−5.389	−2.588	506	HOMO- > LUMO (96%)
PP13	−5.321	−2.454	496	HOMO- > LUMO (95%)

tical potentials. Similarly, the reduction processes are centered on the same part of the molecules so that a reduction at the same potentials is observed.

As observed for **PP8** and **PP9**, **PP12** and **PP13** only differ by the nature of the pendant amine. However, contribution of the nitrogen atom is more limited, and restricted to the LUMO energy level (see Fig. 10). The first oxidation process of **PP12** and **PP13** is centered on the dimethylaminophenyl group of 2-azafluorenone. Since the electron donating moiety is the same for the two molecules, their oxidation potentials are almost similar. The reduction process is located on the 2-azafluorenone part. Considering that only the nitrogen atom of amines contributes to the LUMO level and not the aliphatic part of the amine, **PP12** and **PP13** also reduce at almost similar reduction potentials (See Fig. 23e). While comparing **PP13** and **PP10′** that differ by the length of the conjugated spacer and both possesses an aliphatic pendant amine, similar conclusions than that done for **PP1/PP2** can be established. Notably, a facilitated oxidation of **PP13** due to an elongation of the conjugated spacer is observed. Parallel to this, et due to the delocalization of the LUMO level over the whole molecule, a reduction at more cathodic potentials is observed for **PP10'** (see Table 3 and Fig. 23f).

A final comparison is possible between **PP10** and **PP10'** (See Fig. 23g). The difference between these two molecules is in the aromatization of **PP10′** compared to **PP10**. This aromatization will have an impact on both the HOMO and LUMO distributions over the two molecules. The aromatization of **PP10′** lowers its electron accepting ability compared to **PP10**. Indeed, as evidenced by theoretical calculations, for **PP10′**, the LUMO level is located on the 2-azafluorenone part of the molecule with a contribution to the dimethylaminophenyl group due to the coplanarity of the dimethylaminophenyl group with the naphthalene moiety. Conversely, for **PP10**, contribution of the dimethylaminophenyl group is negligible due to the orthogonality of the dimethylaminophenyl group with the naphthalene moiety (See Figs. 15 and 17). This directly impacts the reduction potential of the molecule, with a reduction occurring at more cathodic potentials for **PP10'** (−1.81 V vs. −1.56 V for **PP10'** and **PP10** respectively). Similarly, major differences can be found for the oxidation potentials. Indeed, for **PP10**, HOMO orbital extends over the whole molecule, including the nitrogen amine of the aliphatic amines.

On the opposite, for **PP10′**, the HOMO is only centered onto the electron-donating group excluding the nitrogen of the pendant amine. As a result of this, oxidation of **PP10′** is more difficult than **PP10** and an increase of the HOMO-LUMO gap is observed for **PP10′** relative to **PP10**. Consequently, a blue-shift of the ICT band is observed for **PP10′** compared to that of **PP10** (See Fig. 18). Finally, a comparison between the theoretical and the electrochemical HOMO and LUMO energy levels can be established. As evidenced in Fig. 24, a good agreement can be found between the theoretical and the experimental values of the HOMO energy levels since a difference lower than 0.5 eV can be determined. Conversely, a greater difference can be found for the LUMO energy levels. As already evidenced in Table 3 for the previous series of **PP1-PP4**, position of the LUMO levels is underestimated by electrochemistry. The same conclusions can thus be established for the present series of dyes **PP6-PP13** and **PP10'**.

4. Conclusions

To conclude, a new series of dihydro-2-azafluorenones and aromatized 2-azafluorenones have been synthesized with a simple one-pot synthesis. Influence of the different parameters such as the amine or the spacer in the aldehydes have also been investigated. By elongating the length of the spacer between the electron donating aldehyde and the electron acceptor, a spontaneous aromatization occurred and lead to the formation of the 2-azafluorenones. Major difference in the photophysical properties of the different dyes have been evidenced. For instance, an easy protonation has been shown by an NMR study in the case of the dihydro-2-azafluorenones. Finally, the synergy between theoretical calculations, UV–visible absorption and photoluminescence spectroscopy, and cyclic voltammetry have allowed to determine the position of the HOMO and the LUMO energy levels as well as the HOMO-LUMO gap for all these new compounds.

Further investigations concerning these different families of compounds need to be carried out. Notably, azafluorenones could be of interest for biological applications such as lipid droplets s-specific imaging [35]. Similarly, push-pull dyes could be used as photoinitiators of polymerization, active materials for solar cells or NLO applications.

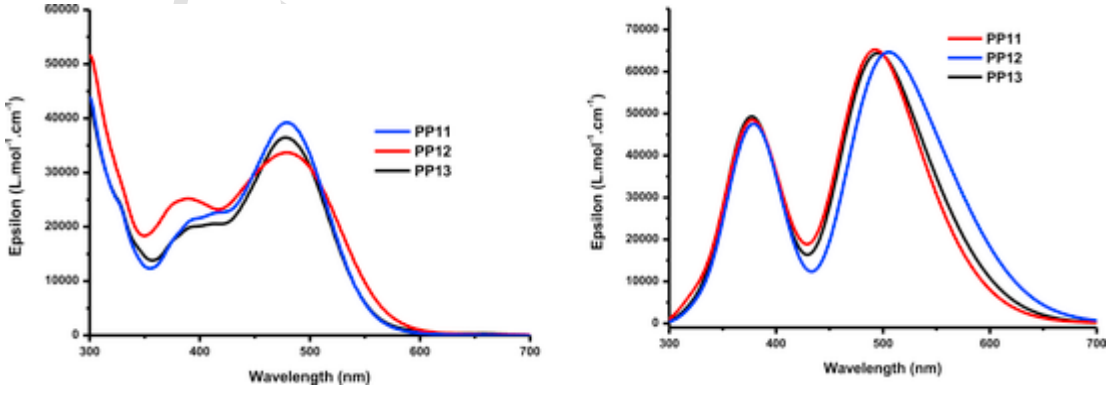

Fig. 16. Comparison between the theoretical (right) an the experimental (left) UV–visible absorption spectra recorded in DMSO for **PP11-PP13**.

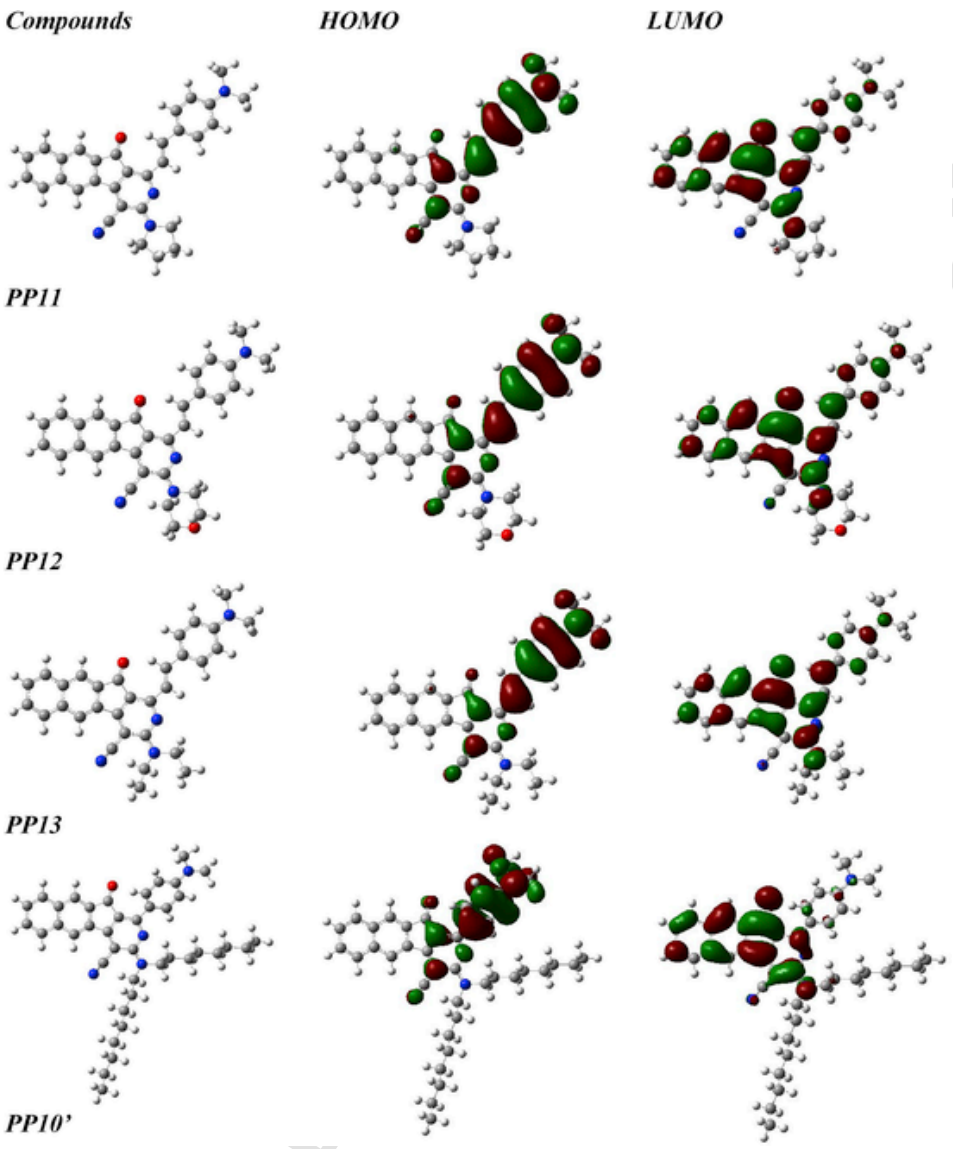

Fig. 17. Optimized geometries and contour plots of the HOMO and LUMO energy levels for the aromatized azafluorenones compounds (**PP11-PP13** and **PP10′**).

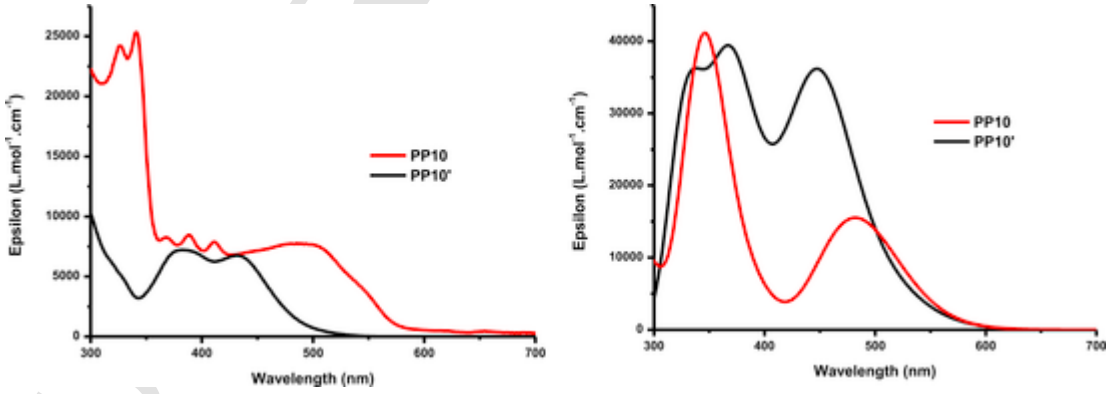

Fig. 18. UV–visible absorption spectra of **PP10** and **PP10′** in chloroform (left) and the theoretical ones (right).

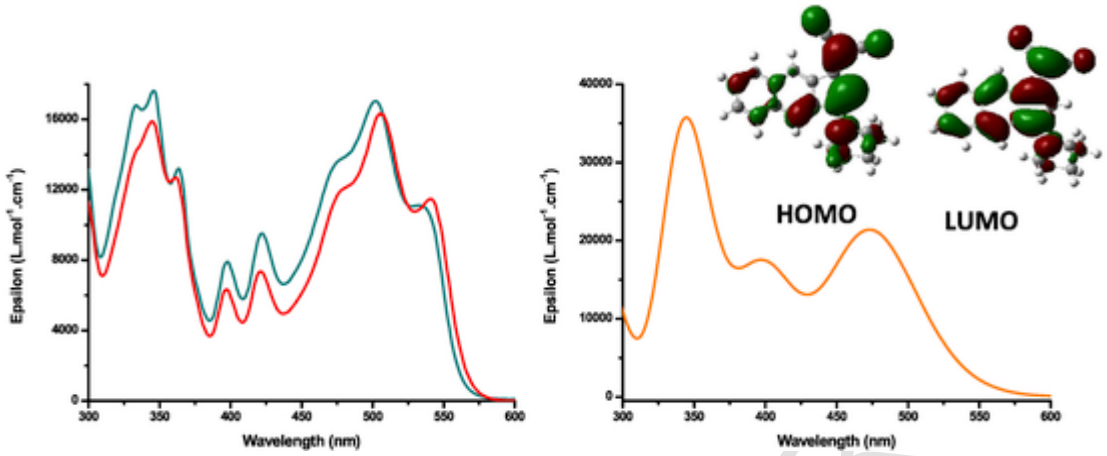

Fig. 19. UV–visible absorption spectrum of **PP5** in DMSO (red) and chloroform (green). (For interpretation of the references to colour in this figure legend, the reader is referred to the Web version of this article.)

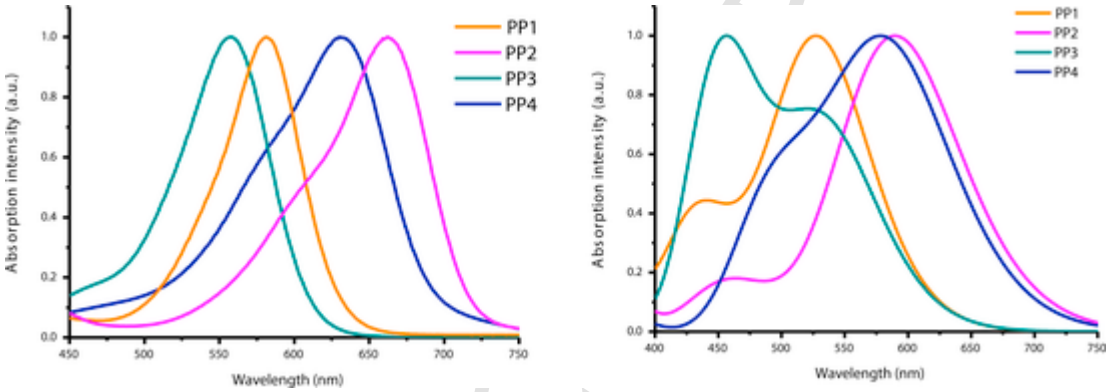

Fig. 20. UV–visible spectra of **PP1-PP4** in chloroform (left) and the theoretical absorption spectra (right).

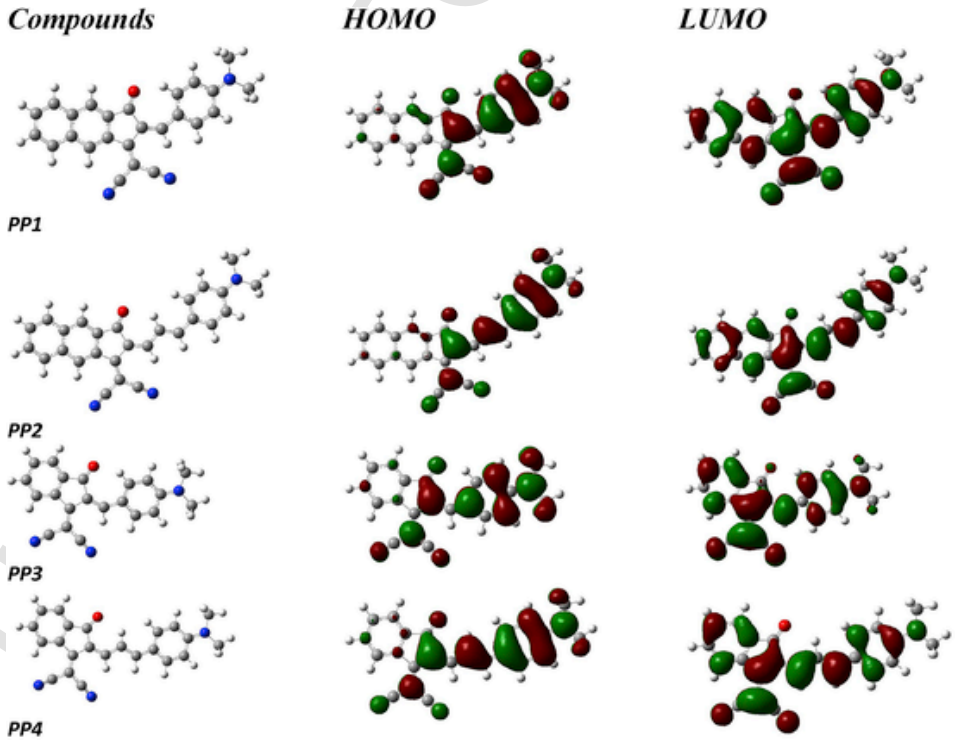

Fig. 21. Optimized geometries and contour plots of the HOMO and LUMO energy levels for **PP1-PP4.**

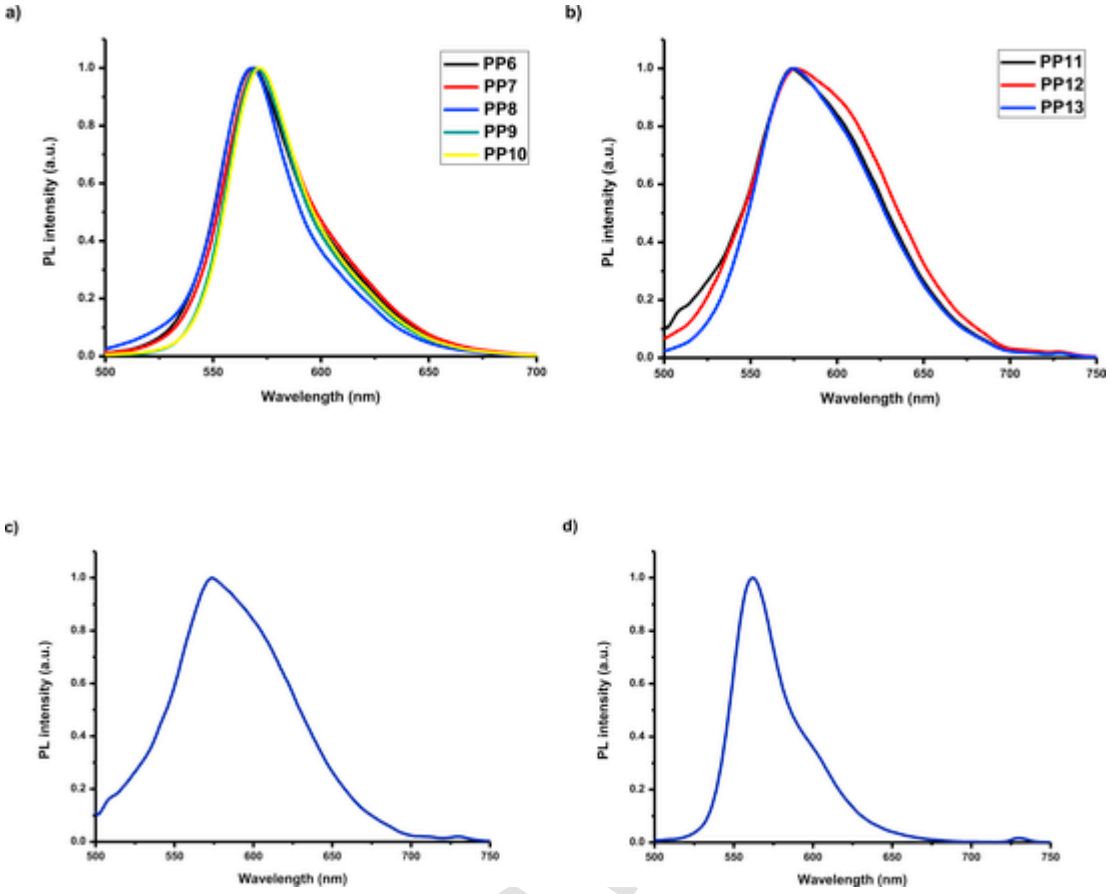

Fig. 22. Photoluminescence spectra of the different dyes recorded in DCM upon excitation at 490 nm. a) **PP6-PP10**, b) **PP11-PP13**, c) **PP10′** and d) **PP5**.

Table 3
Electrochemical characteristics of **PP1-PP13** and values of the electrochemical, optical and theoretical bandgaps of **PP1-PP13**.

Dyes	E_{red} (V)	$E_{red(onset}$ [a] (V)	E_{ox} (V)	$E_{ox(onset)}$ [b] (V)	E_{HOMO} [c] (eV)	E_{LUMO} [c] (eV)	ΔE_{El} (eV)	ΔE_{opt} (eV)	ΔE_{th} (eV)
PP1	−1.26 [irr]	−1.19	0.66	0.56	−5.36	−3.61	1.75	2.13	2.14
PP2	−1.15 [irr]	−1.07	0.42	0.37	−5.17	−3.73	1.44	1.87	1.91
PP3	−1.34 [irr]	−1.27	0.67	0.59	−5.39	−3.53	1.86	2.22	2.20
PP4	−1.21 [irr]	−1.13	0.45	0.39	−5.19	−3.67	1.52	1.97	1.97
PP5	−1.48	−1.43	0.83 [irr]	0.72	−5.52	−3.37	1.82	2.47	3.04
PP6	−1.41	−1.15	0.60 [irr]; 0.32 [irr]	0.23	−5.03	−3.65	1.38	2.50	3.17
PP7	−1.35	−1.18	0.58 [irr]; 0.36 [irr]	0.25	−5.05	−3.62	1.43	2.52	3.18
PP8	−1.84	−1.75	0.63 [irr]; 0.32 [irr]	0.21	−5.01	−3.05	1.96	3.01	3.18
PP9	−1.79	−1.70	0.63 [irr]; 0.30 [irr]	0.21	−5.01	−3.10	1.91	2.52	3.19
PP10	−1.66	−1.62	0.74 [irr]; 0.39 [irr]	0.29	−5.09	−3.18	1.91	2.98	3.19
PP11	−1.74	−1.66	0.64; 0.36 [irr]	0.25	−5.05	−3.14	1.91	2.65	2.90
PP12	−1.63	−1.56	0.65; 0.40 [irr]	0.30	−5.10	−3.24	1.88	2.56	2.80
PP13	−1.72	−1.65	0.63; 0.30 [irr]	0.25	−5.05	−3.15	1.90	2.64	2.87
PP10′	−1.81	−1.75	0.57 [irr]	0.40	−5.20	−3.05	2.15	2.92	3.63

[a] Onset reduction potential versus ferrocene ($E_{Red(onset)}$ vs. Fc).
[b] Onset oxidation potential versus ferrocene ($E_{Ox(onset)}$ vs. Fc).
[c] E_{Homo} and E_{Lumo} were determined from the formulas: E_{HOMO} (eV) = - 4.8 – $E_{Ox(Onset)}$ and E_{LUMO} (eV) = −4.8 – $E_{Red(Onset)}$.

5. Experimental section

5.1. General informations

All reagents and solvents were purchased from Aldrich, Alfa Aesar or TCI Europe and used as received without further purification. Mass spectroscopy was performed by the Spectropole of Aix-Marseille University. ESI mass spectral analyses were recorded with a 3200 QTRAP (Applied Biosystems SCIEX) mass spectrometer. The HRMS mass spectral analysis was performed with a QStar Elite (Applied Biosystems SCIEX) mass spectrometer. Elemental analyses were recorded with a Thermo Finnigan EA 1112 elemental analysis apparatus driven by the Eager 300 software. ^{1}H and ^{13}C NMR spectra were determined at room temperature in 5 mm o.d. tubes on a Bruker Avance 400 spectrometer of the Spectropole: ^{1}H (400 MHz) and ^{13}C (100 MHz). The ^{1}H chemical

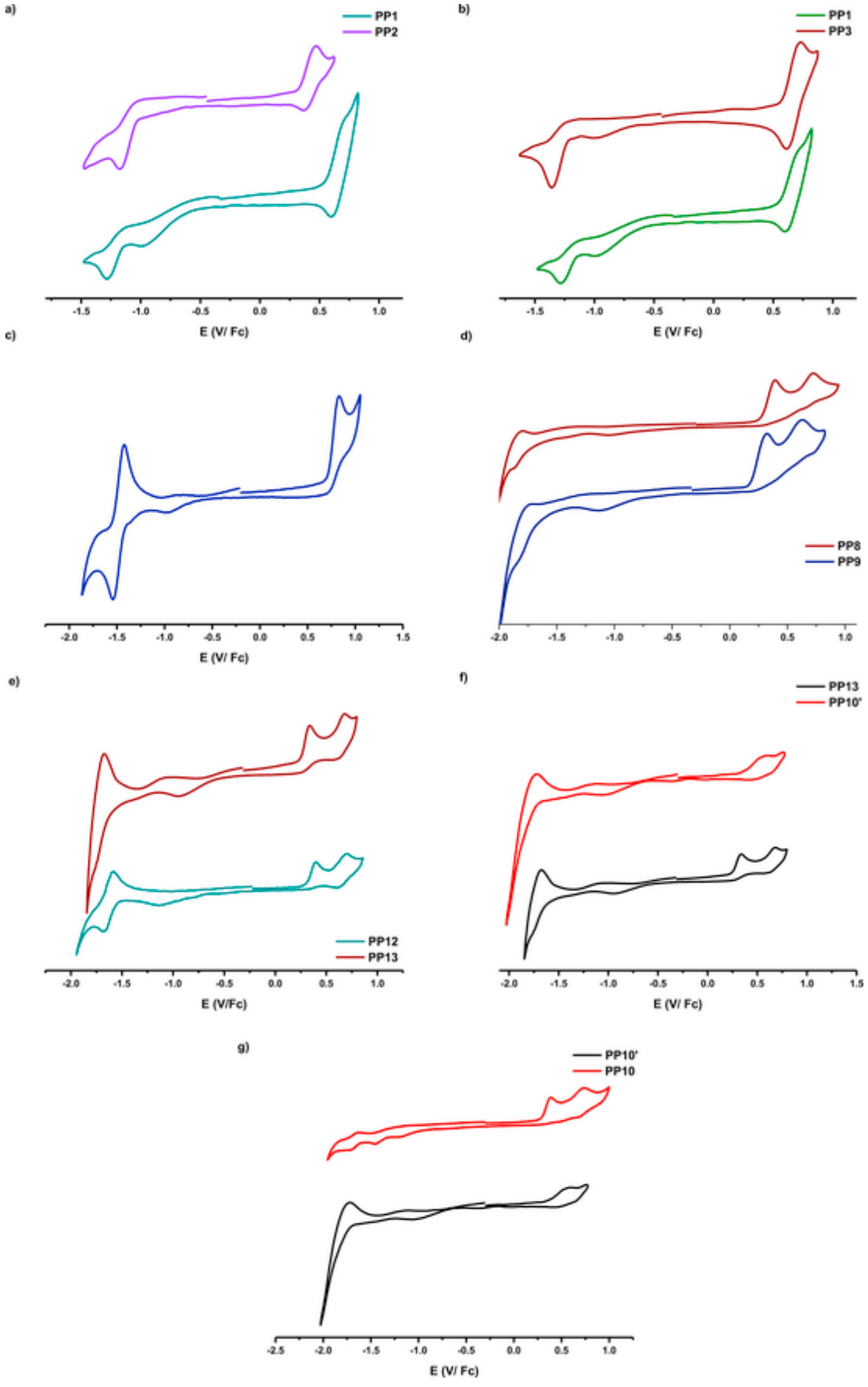
a)
PP1
PP2
E (V/ Fc)
b)
PP1
PP3
E (V/ Fc)
c)
E (V/ Fc)
d)
PP8
PP9
e)
PP12
PP13
E (V/Fc)
f)
PP13
PP10'
E (V/ Fc)
g)
PP10'
PP10
E (V/ Fc)

Fig. 23.

Cyclic voltammograms of a) **PP1** and **PP2**, b) **PP1** and **PP3**, c) **PP5**, d) **PP8** and **PP9**, e) **PP12** and **PP13**, f) **PP10′** and **PP10′**, g) **PP10′** and **PP13** in dichloromethane solutions (10^{-3} M) with tetrabutylammonium perchlorate (0.1 M) as the supporting electrolyte. Scan rate: 100 mV/s.

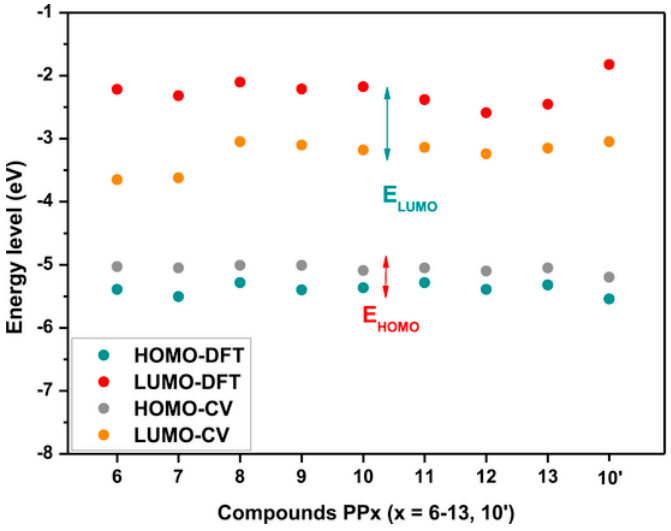

Fig. 24. Comparison between the HOMO and LUMO energy levels determined by cyclic voltammetry and by theoretical calculations for **PP6-PP13** and **PP10′**.

shifts were referenced to the solvent peak $CDCl_3$ (7.26 ppm) and the ^{13}C chemical shifts were referenced to the solvent peak $CDCl_3$ (77 ppm). 2-(3-Oxo-2,3-dihydro-1*H*-inden-1-ylidene)malononitrile [36], 3-(4-(dimethyl-amino)phenyl)acrylaldehyde **ED2** [37] were synthesized as previously reported in the literature, without modification and in similar yields. UV–visible absorption spectra were recorded on a Varian Cary 50 Scan UV Visible Spectrophotometer, with concentration of 5×10^{-3} M, corresponding to diluted solutions. Fluorescence spectra were recorded using a Jasco FP 6200 spectrometer. The electrochemical properties of the investigated compounds were measured in dichloromethane by cyclic voltammetry, scan rate 100 mV/s, with tetrabutylammonium perchlorate (0.1 M) as a supporting electrolyte in a standard one-compartment, three-electrode electrochemical cell under an argon stream using a VSP BioLogic potentiostat. The working, pseudo-reference and counter electrodes were platinum disk (Ø = 1 mm), Ag wire, and Au wire gauze, respectively. Ferrocene was used as an internal standard, and the potentials are referred to the reversible formal potential of this compound. All CV measurements have been acquired upon deaeration of the solutions with argon during 10 min prior to the acquisition of the curves. No measurements have been carried out in glovebox. DFT calculations [38] employing the B3LYP functionals [39,40] and 6-311 + G(d,p) basis set were performed with a Gaussian 09 program [41]. The geometry optimizations for all the molecules were carried out without symmetry constraints and were followed by frequency calculations. The spectroscopic properties of the molecules were calculated by mean of a time dependent density functional theory method (TDDFT) [42–46]. Up to 10 excited states were calculated and the theoretical absorption bands were obtained by considering a band half-width at half-maximum of 0.2 eV [26]. The assignment of electronic transitions for λ_{max} has been determined with GaussSum 3.0 software [47,48].

5.2. Synthesis of the electron acceptors and push-pull dyes

*5.2.1. 2-(3-Oxo-2,3-dihydro-1H-cyclopenta[b]naphthalen-1-ylidene)malononitrile **EA1***

In a dried two-necked 100 mL flask, 1H-cyclopenta[*b*]naphthalene-1,3(2*H*)-dione (1.1 g, 5.6 mmol) and malononitrile (2.2 g, 33.3 mmol) were dissolved in ethanol (25 mL), and then anhydrous sodium acetate (1.84 g) was slowly added while stirring. After stirring for 2 h, the reaction mixture was poured into ice-water, and acidified to pH 1–2 by the addition of concentred hydrochloric acid. The resulting precipitate was collected by filtration and washed with water giving the crude product. It was finally purified with a flash chromatography (eluent: DCM). Yield = 67%. ^1H NMR (400 MHz, $CDCl_3$) δ: 3.85 (s, 2H), 7.79 (dd, 2H, J = 6.2 Hz, J = 3.2 Hz), 8.07–8.19 (m, 2H), 8.49 (s, 1H), 9.19 (s, 1H); ^{13}C NMR (100 MHz, $CDCl_3$) δ: 44.6, 112.3, 112.6, 125.8, 128.1, 130.5, 130.6, 130.7, 130.9, 135.8, 136.3, 136.4, 166.5, 195.3; HRMS (ESI MS) *m/z*: theor: 244.0637 found: 244.0640 ($[M]^{+\cdot}$ detected).

*5.2.2. 1H-cyclopenta[b]naphthalene-1,3(2H)-dione **EA2***

Diethyl naphthalene-2,3-dicarboxylate (10 g, 38.5 mmol) was suspended in dry EtOAc (24 mL) and NaH 95% in oil (2.44 g, 96.4 mmol, 2.5 eq) was added. The reaction mixture was refluxed at 105 °C for 5 h. After cooling, the yellow solid was filtered off and thoroughly washed with a mixture of EtOH–Et_2O 50/50. Treatment of this solid with 200 mL of a 1 M HCl solution under reflux for 1h30 furnished a new solid. After cooling, the solid was filtered off, washed with water and recrystallized in toluene (200 mL) overnight. The product was obtained as a brown solid. Yield = 91%. ^1H NMR (400 MHz, $CDCl_3$) δ: 3.38 (s, 2H), 7.66–7.75 (m, 2H), 8.10–8.13 (m, 2H), 8.52 (s, 2H); ^{13}C NMR (100 MHz, $CDCl_3$) δ: 46.7, 124.3, 129.7, 130.6, 136.4, 138.2, 197.6; HRMS (ESI MS) *m/z*: theor: 196.0524 found: 196.0526 ($[M]^{+\cdot}$ detected).

*5.2.3. General procedure for the synthesis of the push-pull dyes **PP1-PP4***

2-(3-Oxo-2,3-dihydro-1*H*-cyclopenta[*b*]naphthalen-1-ylidene)malononitrile **EA1** (0.62 g, 2.55 mmol) or 2-(3-oxo-2,3-dihydro-1*H*-inden-1-ylidene)malononitrile (0.50 g, 2.55 mmol) and the appropriate aldehyde (4-dimethylaminobenzaldehyde (0.38 g) or 3-(4-(dimethylamino)-phenyl)acrylaldehyde (0.45 g), 2.55 mmol, 1. eq.) were dissolved in absolute ethanol (50 mL) and a few drops of piperidine were added. The reaction mixture was refluxed and progress of the reaction was followed by thin layer chromatography (TLC). After cooling, a precipitate formed. It was filtered off, washed several times with ethanol and dried under vacuum.

*5.2.4. 2-(2-(4-(Dimethylamino)benzylidene)-3-oxo-2,3-dihydro-1H-cyclopenta[b]naphthalen-1-ylidene)malononitrile **PP1***

Yield = 68%. ^1H NMR (400 MHz, $CDCl_3$) δ: 3.23 (s, 6H), 6.77 (d, 2H, J = 9.2 Hz), 7.65–7.67 (m, 2H), 8.01–8.03 (m, 1H), 8.06–8.08 (m, 1H), 8.32 (s, 1H), 8.44 (d, 2H, J = 9.2 Hz), 8.57 (s, 1H), 9.14 (s, 1H); HRMS (ESI MS) *m/z*: theor: 376.1444 found: 376.1442 ($[M+H]^+$ detected); Anal. Calc. for $C_{25}H_{17}N_3O$: C, 80.0; H, 11.2; O, 4.3; Found: C, 79.8; H, 11.3; O, 4.5%

*5.2.5. 2-(-2-(-3-(4-(Dimethylamino)phenyl)allylidene)-3-oxo-2,3-dihydro-1H-cyclopenta[b]naphthalen-1-ylidene)malononitrile **PP2***

Yield = 44%. ^1H NMR (400 MHz, $CDCl_3$) δ: 3.15 (s, 6H), 6.72 (d, 2H, J = 9.0 Hz), 7.46 (d, 1H, J = 14.8 Hz), 7.66–7.68 (m, 3H),

8.02–8.08 (m, 2H), 8.32 (s, 1H), 8.61 (d, 1H, J = 11.9 Hz), 8.78 (dd, 1H, J = 12.0 Hz, J = 14.6 Hz), 9.15 (s, 1H); HRMS (ESI MS) *m/z*: theor: 402.1601 found: 402.1600 ($[M+H]^+$ detected); Anal. Calc. for $C_{27}H_{19}N_3O$: C, 80.8; H, 4.8; O, 4.0; Found: C, 80.6; H, 4.6; O, 4.1%

*5.2.6. 2-(2-(4-(Dimethyl-amino)benzylidene)-3-oxo-2,3-dihydro-1H-inden-1-ylidene)malononitrile **PP3***

Yield = 55%. ^{1}H NMR (400 MHz, $CDCl_3$) δ: 3.19 (s, 6H), 6.74 (d, 2H, J = 9.2 Hz), 7.65–7.72 (m, 2H), 7.84–7.86 (m, 1H), 8.37 (d, 2H, J = 9.2 Hz), 8.62 (s, 1H), 8.64 (d, 1H, J = 8.0 Hz); ^{13}C NMR (100 MHz, $CDCl_3$) δ: 40.2, 67.3, 111.5, 115.2, 115.4, 121.9, 122.6, 123.4, 124.7, 133.9, 134.4, 137.3, 139.1, 139.6, 148.2, 154.7, 163.5, 187.4; HRMS (ESI MS) *m/z*: theor: 326.3785 found: 326.3788 ($[M+H]^+$ detected).

*5.2.7. 2-(2-(3-(4-(Dimethylamino)phenyl)allylidene)-3-oxo-2,3-dihydro-1H-inden-1-ylidene)malononitrile **PP4** [28]*

Yield = 45%. ^{1}H NMR (400 MHz, $CDCl_3$) δ: 3.12 (s, 6H), 6.70 (d, 2H, J = 8.9 Hz), 7.38 (d, 1H, J = 14.7 Hz), 7.62 (d, 2H, J = 8.9 Hz), 7.61–7.71 (m, 2H), 7.84–7.87 (m, 1H), 8.50 (d, 1H, J = 11.9 Hz), 8.61–8.68 (m, 2H); ^{13}C NMR (100 MHz, $CDCl_3$) δ: 40.1, 67.5, 112.1, 115.1, 115.2, 120.2, 122.5, 123.3, 123.9, 125.1, 130.4, 132.5, 133.9, 134.5, 137.3, 139.9, 149.0, 153.3, 156.1, 160.2, 189.7; HRMS (ESI MS) *m/z*: theor: 352.1444 found: 352.1441 ($[M+H]^+$ detected).

*5.2.8. 2-(3-(Piperidin-1-yl)-1H-cyclopenta[b]naphthalen-1-ylidene)malononitrile **PP5***

4-Dimethylaminobenzaldehyde **ED1** (0.77 g, 5.15 mmol) and 2-(3-oxo-2,3-dihydro-1*H*-cyclopenta[*b*]naphthalen-1-ylidene)malononitrile **EA1** (1.25 g, 5.15 mmol) were suspended in 20 mL absolute ethanol and a few drops of piperidine were added. Immediately, the solution turned deep red. The flask was introduced in an oil bath preheated at 90 °C. After 15 min, the reaction was ended (TLC control). During that time, an extremely insoluble precipitate was formed. After cooling, the precipitate was filtered off, washed several times with ethanol and ether, and dried under vacuum. Yield = 86%; ^{1}H NMR (400 MHz, $CDCl_3$) δ: 1.85 (brs, 6H), 3.86 (brs, 4H), 5.87 (s, 1H), 7.52–7.57 (m, 2H), 7.77–7.89 (m, 3H), 8.57 (s, 1H); ^{13}C NMR (100 MHz, $CDCl_3$) δ: ^{13}C NMR (75 MHz, $CDCl_3$) δ 23.8, 26.1, 51.5, 56.9, 103.1, 116.9, 117.0, 123.7, 124.3, 128.40, 128.41, 129.5, 129.8, 133.1, 133.3, 133.5, 134.3, 161.8, 162.6; HRMS (ESI MS) *m/z*: theor: 312.1495 found: 312.1492 ($[M]^{+\cdot}$ detected).

*5.3. General procedure for the synthesis of the push-pull dyes **PP6-PP13***

The selected aldehyde (1,64 mmol, 1 eq.) and **EA1** (1.64 mmol, 1 eq.) were introduced in a preheated solution of ethanol (40 mL). the selected amine (0.5 mL) was added in the former solution while boiling. Monitoring of the reaction was done by TLC and the solution was approximately refluxed for 30 min. Depending of the amine, upon cooling, a precipitate formed in most of the time. This solid was filtered off and discarded. Addition of Et_2O in the filtrate furnished a precipitate that was filtered off, washed with ether and dried under vacuum. In the case that no precipitation occurred upon addition of ether, the solvent was removed under reduced pressure and the residue was purified by column chromatography (SiO_2).

*5.3.1. 1-(4-(Dimethylamino)phenyl)-11-oxo-3-(piperidin-1-yl)-2,11-dihydro-1H-benzo[5,6]indeno[2,1-c]pyridine-4-carbonitrile **PP6***

Yield = 14%. ^{1}H NMR (400 MHz, Acetone-d_6) δ: 1.68–1.80 (m, 6H), 2.90 (s, 6H), 3.58–3.87 (m, 4H), 5.59 (d, 2H, J = 4.8 Hz), 6.71 (d, 2H, J = 8.8 Hz), 7.23 (d, 2H, J = 8.8 Hz), 7.48–7.61 (m, 2H), 7.74 (s, 1H), 7.93 (dd, 2H, J = 13.7 Hz, J = , 7.5 Hz), 8.20 (s, 1H); ^{1}H NMR (400 MHz, $CDCl_3$) δ: 1.72–1.75 (m, 6H), 2.90 (s, 6H), 3.50–3.57 (m, 2H), 3.62–3.68 (m, 2H), 5.57–5.60 (m, 2H), 6.67 (d, 2H, J = 8.5 Hz), 7.25 (d, 2H, J = 8.5 Hz), 7.40–7.48 (m, 2H), 7.71 (s, 1H), 7.77 (d, 1H, J = 7.6 Hz), 7.82 (d, 1H, J = 7.6 Hz), 8.18 (s, 1H); ^{13}C NMR (100 MHz, $CDCl_3$): 25.4, 40.2, 40.4, 49.8, 54.2, 80.2, 110.9, 112.4, 120.5, 120.9, 123.5, 124.1, 127.2, 127.9, 128.4, 129.5, 130.1, 131.9, 133.3, 133.7, 134.8, 136.2, 153.6, 157.3, 160.1, 160.2, 187.2; HRMS (ESI MS) *m/z*: theor: 461.2336 found: 461.2333 ($[M+H]^+$ detected).

*5.3.2. 1-(4-(Dimethylamino)phenyl)-3-morpholino-11-oxo-2,11-dihydro-1H-benzo[5,6]indeno[2,1-c]pyridine-4-carbonitrile **PP7***

Yield = 79%. ^{1}H NMR (400 MHz, $CDCl_3$) δ: 2.92 (s, 6H), 3.47–3.52 (m, 4H), 3.72–3.77 (m, 4H), 5.42 (brs, 1H), 5.63 (d, 1H, J = 3.9 Hz), 6.68 (d, 2H, J = 8.5 Hz), 7.25 (d, 2H, J = 8.5 Hz), 7.44–7.52 (m, 2H), 7.74 (s, 1H), 7.79 (d, 1H, J = 7.8 Hz), 7.84 (d, 1H, J = 7.8 Hz), 8.16 (s, 1H); ^{1}H NMR (400 MHz, DMSO-d_6) δ: 2.85 (s, 6H), 3.44–3.54 (m, 2H), 3.69–3.78 (m, 6H), 5.49 (s, 1H), 6.68 (d, 2H, J = 8.9 Hz), 7.12 (d, 2H, J = 8.9 Hz), 7.50–7.58 (m, 2H), 7.78 (s, 1H), 7.89 (d, 1H, J = 8.6 Hz), 7.98 (d, 1H, J = 8.6 Hz), 8.04 (s, 1H), 8.97 (s, 1H); ^{13}C NMR (100 MHz, DMSO-d_6) δ: 48.0, 49.1, 51.5, 59.3, 65.9, 112.4, 117.5, 119.0, 119.8, 120.2, 127.2, 128.0, 129.0, 129.8, 129.9, 131.9, 133.3, 133.6, 134.4, 135.3, 149.9, 153.3, 160.2, 185.9; HRMS (ESI MS) *m/z*: theor: 463.2129 found: 463.2126 ($[M+H]^+$ detected).

*5.3.3. 1-(4-(Dimethylamino)phenyl)-11-oxo-3-(pyrrolidin-1-yl)-2,11-dihydro-1H-benzo[5,6]indeno[2,1-c]pyridine-4-carbonitrile **PP8***

Yield = 36%. ^{1}H NMR (400 MHz, DMSO-d_6) δ: 1.85–1.95 (m, 2H), 1.99–2.08 (m, 2H), 2.85 (s, 6H), 3.62–3.70 (m, 2H), 3.71–3.80 (m, 2H), 5.44 (d, 1H, J = 3.6 Hz), 6.68 (d, 2H, J = 8.8 Hz), 7.16 (d, 2H, J = 8.8 Hz), 7.49–7.55 (m, 2H), 7.73 (s, 1H), 7.86 (d, 1H, J = 7.0 Hz), 7.96 (d, 1H, J = 7.0 Hz), 8.12 (d, 1H, J = 4.0 Hz), 8.16 (s, 1H); ^{13}C NMR (125 MHz, DMSO-d_6) δ: 24.9, 49.9, 51.7, 56.0, 58.4, 108.8, 112.4, 119.3, 119.8, 121.3, 126.6, 127.0, 127.7, 129.2, 129.6, 130.9, 133.5, 134.2, 134.4, 135.5, 150.0, 153.4, 155.5, 185.1; HRMS (ESI MS) *m/z*: theor: 447.2179 found: 447.2179 ([M] + . detected).

*5.3.4. 3-(Diethylamino)-1-(4-(dimethylamino)phenyl)-11-oxo-2,11-dihydro-1H-benzo[5,6]indeno[2,1-c]pyridine-4-carbonitrile **PP9***

Yield = 10%. ^{1}H NMR (400 MHz, $CDCl_3$) δ: 1.19 (t, 6H, J = 6.9 Hz), 2.84 (s, 6H), 3.54–3.69 (m, 4H), 5.43 (s, 1H), 6.68 (d, 2H, J = 8.7 Hz), 7.12 (d, 2H, J = 8.6 Hz), 7.49–7.56 (m, 2H), 7.74 (s, 1H), 7.86 (d, 1H, J = 7.4 Hz), 7.96 (d, 1H, J = 7.4 Hz), 8.14 (s, 1H), 8.26 (s, 1H); ^{13}C NMR (100 MHz, $CDCl_3$) δ: 13.4, 40.0, 44.8, 51.8, 58.4, 112.3, 117.1, 119.4, 120.0, 120.5, 126.6, 127.1, 127.9, 129.1, 129.8, 130.0, 133.5, 134.0, 134.5, 135.4, 149.9, 153.6, 158.0, 185.3; HRMS (ESI MS) *m/z*: theor: 449.2336 found: 449.2334 ($[M+H]^+$ detected).

*5.3.5. 1-(4-(Dimethylamino)phenyl)-3-(dioctylamino)-11-oxo-2,11-dihydro-1H-benzo[5,6]indeno[2,1-c]pyridine-4-carbonitrile **PP10***

Yield = 5%. ^{1}H NMR (400 MHz, acetone-d_6) δ: 0.85 (t, 6H, J = 6.7 Hz), 1.26–1.29 (m, 20H), 1.70 (qt, 4H, J = 7.5 Hz), 2.90 (s, 6H), 3.49–3.56 (m, 2H), 3.79–3.86 (m, 2H), 5.51 (d, 1H, J = 4.5 Hz), 6.68 (d, 2H, J = 8.9 Hz), 7.22 (d, 2H, J = 8.9 Hz), 7.50–7.55 (m, 3H), 7.72 (s, 1H), 7.92 (t, 2H, J = 7.1 Hz), 8.29 (s, 1H); ^{13}C NMR (100 MHz, acetone-d_6) δ: 14.4, 23.3, 27.2, 28.9, 29.3, 29.97, 29.99, 32.6, 40.6, 51.8, 53.9, 60.6, 113.3, 118.9, 120.7, 120.9, 127.8, 128.0, 128.6, 130.1, 130.7, 131.3, 134.9, 135.5, 136.2, 137.2, 151.4, 154.6, 160.3, 187.0; HRMS (ESI MS) *m/z*: theor: 617.4214 found: 617.4206 ($[M+H]^+$ detected).

*5.3.6. 1-(4-(Dimethylamino)phenyl)-3-(dioctylamino)-11-oxo-11H-benzo[5,6]indeno[2,1-c]pyridine-4-carbonitrile **PP10'***

Yield = 25%. ^{1}H NMR (400 MHz, $CDCl_3$) δ: 0.90 (t, 6H, J = 6.5 Hz), 1.31–1.50 (m, 20H), 1.82 (qt, 4H, J = 6.9 Hz), 3.07 (s, 6H), 3.82 (t, 4H, J = 7.7 Hz), 4.26-4.20 (m, 1H), 6.76 (d, 2H,

J = 9.0 Hz), 7.53–7.58 (m, 2H), 7.91–7.98 (m, 2H), 8.04 (d, 2H, J = 9.0 Hz), 8.16 (s, 1H), 8.89 (s, 1H); ^{13}C NMR (100 MHz, $CDCl_3$) δ: 14.1, 22.6, 26.8, 28.6, 29.3, 29.4, 29.7, 31.8, 40.1, 51.2, 110.6, 116.5, 118.7, 123.7, 124.1, 124.2, 128.0, 128.5, 129.4, 130.0, 131.9, 133.6, 133.8, 134.6, 136.0, 152.2, 158.2, 159.6, 160.5, 187.1; HRMS (ESI MS) m/z: theor: 615.8855 found: 615.8853 ($[M+H]^+$ detected).

5.3.7. (E)-1-(4-(Dimethylamino)styryl)-11-oxo-3-(pyrrolidin-1-yl)-11H-benzo[5,6]indeno[2,1-c]pyridine-4-carbonitrile ***PP11***

Yield = 18%. ^{1}H NMR (400 MHz, $CDCl_3$) δ: 2.06–2.10 (m, 4H), 3.05 (s, 6H), 4.04–4.06 (m, 4H), 6.71 (d, 2H, J = 8.8 Hz), 7.56–7.60 (m, 2H), 7.62 (d, 2H, J = 8.8 Hz), 7.94–8.01 (m, 2H), 8.03 (s, 1H), 8.17–8.22 (m, 2H), 8.79 (s, 1H); ^{13}C NMR (100 MHz, $CDCl_3$) δ: 25.5, 40.2, 49.6, 81.1, 111.9, 116.3, 118.0, 118.8, 123.8, 123.9, 124.4, 128.0, 128.4, 130.0, 130.2, 133.7, 134.1, 134.6, 136.0, 139.8, 151.3, 156.5, 188.5; HRMS (ESI MS) m/z: theor: 471.2179 found: 471.2181 ($[M+H]^+$ detected).

5.3.8. (E)-1-(4-(Dimethylamino)styryl)-3-morpholino-11-oxo-11H-benzo[5,6]indeno[2,1-c]pyridine-4-carbonitrile ***PP12***

Yield = 6%. ^{1}H NMR (400 MHz, $CDCl_3$) δ: 3.05 (s, 6H), 3.93–4.00 (m, 8H), 6.70 (d, 2H, J = 8.6 Hz), 7.56–7.61 (m, 4H), 7.93–7.98 (m, 3H), 8.14 (d, 1H, J = 15.5 Hz), 8.17 (s, 1H), 8.69 (s, 1H); ^{13}C NMR (100 MHz, $CDCl_3$) δ: 40.2, 48.6, 48.8, 84.0, 110.8, 111.9, 117.5, 117.8, 118.0, 123.9, 124.0, 124.6, 128.3, 128.9, 130.1, 130.2, 130.4, 132.1, 133.5, 133.6, 134.7, 136.0, 140.8, 151.6, 156.1, 188.9; HRMS (ESI MS) m/z: theor: 487.2129 found: 487.2127 ($[M+H]^+$ detected).

5.3.9. (E)-3-(Diethylamino)-1-(4-(dimethylamino)styryl)-11-oxo-11H-benzo[5,6]indeno[2,1-c]pyridine-4-carbonitrile ***PP13***

Yield = 5%. ^{1}H NMR (400 MHz, $CDCl_3$) δ: 1.37 (t, 3H, J = 6.9 Hz), 1.39 (t, 3H, J = 6.9 Hz), 2.98 (s, 6H), 3.85 (q, 2H, J = 6.9 Hz), 3.87 (q, 2H, J = 6.9 Hz), 6.65 (d, 2H, J = 8.2 Hz), 7.51–7.56 (m, 4H), 7.88–7.92 (m, 3H), 8.11 (d, 2H, J = 8.2 Hz), 8.78 (s, 1H); ^{13}C NMR (400 MHz, $CDCl_3$) δ: 13.8, 29.7, 40.2, 45.2, 112.0, 116.6, 118.1, 118.7, 124.0, 124.1, 124.3, 128.1, 128.6, 130.0, 130.1, 130.2, 132.1, 133.0, 133.1, 133.8, 134.1, 134.6, 136.0, 140.0, 151.4, 156.2, 188.2; HRMS (ESI MS) m/z: theor: 473.2336 found: 473.2339 ($[M+H]^+$ detected).

Author contribution statement

C.P., G.N. and F.D. conceived this work. C.P. and F.D. designed and executed the experimental work, analyzed the data and discussed the results. C.P. and G.N. realized the chemical characterizations and the photophysical analysis of the compounds. S.D. solved the crystal structures. S.P. carried out the theoretical calculations. T.-T. B. and P.-H. supervised the electrochemistry experiments. M.N. and D.G. did a critical review of the manuscript. C.P., G.N. and F.D. contributed to writing and editing the manuscript.

Declaration of competing interest

The authors declare no conflict of interest.

Acknowledgements

The authors thank Aix Marseille University and The Centre National de la Recherche (CNRS) for financial supports. The Agence Nationale de la Recherche (ANR agency) is acknowledged for its financial support through the PhD grants of Corentin Pigot (ANR-17-CE08-0010 DUALITY project) and Guillaume Noirbent (ANR-17-CE08-0054 VISICAT project). Said Aboudou is acknowledged as Master student from the Master *Nanosciences and Nanotechnologies* of Aix Marseille University for its contribution to the photophysical characterizations of the dyes.

Appendix A. Supplementary data

Supplementary data to this article can be found online at https://doi.org/10.1016/j.dyepig.2020.108182.

References

[1] B. Carlotti, A. Cesaretti, G. Cacioppa, F. Elisei, I. Odak, I. Škorić, et al Fluorosolvatochromism and hyperpolarizability of one-arm and two-arms nitro-compounds bearing heterocyclic rings. J Photochem Photobiol A Chem 2019;368:190–199.
[2] A. Cesaretti, C. Bonaccorso, F. Elisei, C.G. Fortuna, L. Mencaroni, A. Spalletti Photoinduced intramolecular charge transfer and hyperpolarizability coefficient in push-pull pyridinium salts with increasing strength of the acceptor group. ChemPlusChem 2018;83:1021–1031.
[3] H. Motiei, A. Jafari, R. Naderali Third-order nonlinear optical properties of organic azo dyes by using strength of nonlinearity parameter and Z-scan technique. Opt Laser Technol 2017;88:68–74.
[4] R.M. El-Shishtawy, F.A.M. Al-Zahrani, S.M. Afzal, M.A.N. Razvi, Z.M. Al-amshany, A.H. Bakryc, et al Linear and nonlinear optical properties of a new dimethine cyanine dye derived from phenothiazine. RSC Adv 2016;6:91546–91556.
[5] F. Chaumel, H. Jiang, A. Kakkar Sol-gel materials for second-order nonlinear optics. Chem Mater 2001;13:3389–3395.
[6] S. Matsumoto, K.-I. Kubodera, T. Kurihara, T. Kaino Nonlinear optical properties of an azo dye attached polymer. Appl Phys Lett 1987;51:1–2.
[7] D.G. Kim, H.C. Jin, R.D. Maduwu, S.A. Salma, D.K. Moon, J.H. Kim Synthesis of new conjugated small-molecule-dyes based on 2-(2-methyl-4H-chromen-4-ylidene) malononitrile as the electron-withdrawing group and their application in photovoltaic devices. Dyes Pigments 2019;163:660–666.
[8] P. Blanchard, C. Malacrida, C. Cabanetos, J. Roncali, S. Ludwigs Triphenylamine and some of its derivatives as versatile building blocks for organic electronic applications. Polym Int 2019;68:589–606.
[9] V. Malytskyi, J.-J. Simon, L. Patrone, J.-M. Raimundo Thiophene-based push–pull chromophores for small molecule organic solar cells (SMOSCs). RSC Adv 2015;5:354–397.
[10] C.-P. Lee, C.-T. Li, K.-C. Ho Use of organic materials in dye-sensitized solar cells. Mater Today 2017;20:267–283.
[11] C.-P. Lee, R.Y.-Y. Lin, L.-Y. Lin, C.-T. Li, T.-C. Chu, S.-S. Sun, et al Recent progress in organic sensitizers for dye-sensitized solar cells. RSC Adv 2015;5:23810–23825.
[12] A. Mishra, M.K.R. Fischer, P. Bäuerle Metal-free organic dyes for dye-sensitized solar cells: from structure: property relationships to design rules. Angew Chem Int Ed 2009;48:2474–2499.
[13] Y. Farré, M. Raissi, A. Fihey, Y. Pellegrin, E. Blart, D. Jacquemin, et al Synthesis and properties of new benzothiadiazole-based push-pull dyes for p-type dye sensitized solar cells. Dyes Pigments 2018;148:154–166.
[14] S. Forget, S. Chenais, D. Tondelier, B. Geffroy, I. Gozhyk, M. Lebental, et al Red-emitting fluorescent organic light emitting diodes with low sensitivity to self-quenching. J Appl Phys 2010;108:064509.
[15] M.-A. Tehfe, F. Dumur, B. Graff, F. Morlet-Savary, D. Gigmes, J.-P. Fouassier, et al Push-pull (thio)barbituric acid derivatives in dye photosensitized radical and cationic polymerization reactions under 457/473 nm Laser beams or blue LEDs. Polym Chem 2013;4:3866–3875.
[16] M.-A. Tehfe, F. Dumur, B. Graff, F. Morlet-Savary, D. Gigmes, J.-P. Fouassier, et al New push-pull dyes derived from Michler's ketone for polymerization reactions upon visible lights. Macromolecules 2013;46:3761–3770.
[17] H. Mokbel, S. Telitel, F. Dumur, L. Vidal, D.-L. Versace, M.-A. Tehfe, et al Photoinitiating systems of polymerization and in-situ incorporation of metal nanoparticles in polymer matrixes upon visible lights: push-pull malonate and malonitrile based dyes. Polym Chem 2013;4:5679–5687.
[18] P. Xiao, M. Frigoli, F. Dumur, B. Graff, D. Gigmes, J.-P. Fouassier, et al Julolidine or fluorenone based push-pull dyes for polymerization upon soft polychromatic visible light or green light. Macromolecules 2014;47:106–112.
[19] M.-A. Tehfe, F. Dumur, B. Graff, D. Gigmes, J.-P. Fouassier, J. Lalevée Blue-to-red light sensitive push-pull structured photoinitiators: indanedione derivatives for radical and cationic photopolymerization reactions. Macromolecules 2013;46:3332–3341.
[20] O.F. Luna, J. Gomez, C. Cárdenas, F. Albericio, S.H. Marshall, F. Guzmán Deprotection reagents in Fmoc solid phase peptide synthesis: moving away from piperidine? Molecules 2016;21:1542.
[21] T. Landmesser, A. Linden, H.-J. Hansen A novel route to 1-substituted 3-(dialkylamino)-9-oxo-9*H*-indeno[2,1-*c*]-pyridine-4-carbonitriles. Helv Chim Acta 2008;91:265–284.
[22] S. Helmy, S. Oh, F.A. Leibfarth, C.J. Hawker, J. Read de Alaniz Design and synthesis of donor–acceptor Stenhouse adducts: a visible light photoswitch derived from furfural. J Org Chem 2014;79:11316–11329.
[23] M. Gao, H. Su, Y. Lin, X. Ling, S. Li, A. Qin, et al Photoactivatable aggregation-induced emission probes for lipid droplets-specific live cell imaging. Chem Sci 2017;8:1763–1768.
[24] M. Chang, Y. Wang, Y.-Q.-Q. Yi, X. Ke, X. Wan, C. Li, et al Fine-tuning the side-chains of non-fullerene small molecule acceptors to match with appropriate polymer donors. J Mater Chem 2018;6:8586–8594.

[25] R. Li, G. Liu, M. Xiao, X. Yang, X. Liu, Z. Wang, et al Non-fullerene acceptors based on fused-ring oligomers for efficient polymer solar cells via complementary light-absorption. J Mater Chem 2017;5:23926–23936.
[26] H. Feng, N. Qiu, X. Wang, Y. Wang, B. Kan, X. Wan, et al An A-D-A type small-molecule electron acceptor with end-extended conjugation for high performance organic solar cells. Chem Mater 2017;29:7908–7917.
[27] A. Singh, C.-K. Lim, Y.-D. Lee, J.-H. Maeng, S. Lee, J. Koh, et al Tuning solid-state fluorescence to the near-infrared: a combinatorial approach to discovering molecular nanoprobes for biomedical imaging. ACS Appl Mater Interfaces 2013;5:8881–8888.
[28] G. Meshulam, G. Berkovic, Z. Kotler, A. Ben-Asuly, R. Mazor, L. Shapiro, et al 2-D effects in the second-order optical nonlinearity of organic molecules incorporating carbazole. Synth Met 2000;115:219–223.
[29] D.R. Buckle, N.J. Morgan, J.W. Ross, H. Smith, B.A. Spicer Antiallergic activity of 2-nitroindan-1, 3-diones. J Med Chem 1973;16:1334–1339.
[30] C. Pigot, G. Noirbent, T.-T. Bui, S. Péralta, D. Gigmes, M. Nechab, et al Push-pull chromophores based on the naphthalene scaffold: potential candidates for optoelectronic applications. Materials 2019;12:1342.
[31] H. Feng, N. Qiu, X. Wang, Y. Wang, B. Kan, X. Wan, et al An A-D-A type small-molecule electron acceptor with end-extended conjugation for high performance organic solar cells. Chem Mater 2017;29:7908–7917.
[32] Z. Chen, T.M. Swager Synthesis and characterization of fluorescent acenequinones as dyes for guest-host liquid crystal displays. Org Lett 2007;9:997–1000.
[33] F. Dumur, C.R. Mayer, E. Dumas, F. Miomandre, M. Frigoli, F. Sécheresse New chelating stilbazonium-like dyes from Michler's ketone. Org Lett 2008;10:321–324.
[34] J. Pomrnerehne, H. Vestweber, W. Gun, R.E. Muhrt, H. Bassler, M. Porsch, et al Efficient two layer LEDs on a polymer blend basis. Adv Mater 1995;7:551–554.
[35] T.K. Fam, A.S. Klymchenko, M. Collot Recent advances in fluorescent probes for lipid droplets. Materials 2018;11. 1768–1-1768-19.
[36] Y. Cui, H. Ren, J. Yu, Z. Wang, G. Qian An indanone-based alkoxysilane dye with second order nonlinear optical properties. Dyes Pigments 2009;81:53–57.
[37] I. Malina, V. Kampars, B. Turovska, S. Belyakov Novel green-yellow-orange-red light emitting donor-p-acceptor type dyes based on 1,3-indandione and dimedone moieties. Dyes Pigments 2017;139:820–830.
[38] W. Kohn, L.J. Sham Self-consistent equations including exchange and correlation effects. Phys Rev 1965;140:A1133–A1138.
[39] C. Lee, W. Yang, R.G. Parr Development of the Colle-Salvetti correlation-energy formula into a functional of the electron density. Phys Rev B Condens Matter Mater Phys 1988;37:785–789.
[40] A.D. Becke Density-functional thermochemistry. III. The role of exact exchange. J Chem Phys 1993;98:5648–5652.
[41] M.J. Frisch, G.W. Trucks, H.B. Schlegel, G.E. Scuseria, M.A. Robb, J.R. Cheeseman, et al Petersson GA and others, Gaussian 09 (Revision B.01). Wallingford, CT: Gaussian, Inc.; 2009.
[42] E. Gross, W. Kohn Local density-functional theory of frequency-dependent linear response. Phys Rev Lett 1985;55:2850–2852.
[43] E. Runge, E.K.U. Gross Density-functional theory for time-dependent systems. Phys Rev Lett 1984;52:997–1000.
[44] E.K.U. Gross, W. Kohn Density functional theory of many-fermion systems. Adv Quant Chem 1990;21:1–405.
[45] R. Bauernschmitt, R. Ahlrichs Treatment of electronic excitations within the adiabatic approximation of time dependent density functional theory. Chem Phys Lett 1996;256:454–464.
[46] M.E. Casida, C. Jamorski, K.C. Casida, D.R. Salahub Molecular excitation energies to high-lying bound states from time-dependent density functional response theory: characterization and correction of the time dependent local density approximation ionization threshold. J Chem Phys 1998;108:4439–4449.
[47] R. Dennington, T. Keith, J. Millam GAUSSVIEW (version 5). Shawnee Mission KS: Semichem Inc.; 2009.
[48] N.M. O'Boyle, A.L. Tenderholt, K.M. Langner cclib: a library for package-independent computational chemistry algorithms. J Comput Chem 2008;29:839–845.